bodies clearly demonstrate a Q79-dependent decrease in H3 and H4 acetylation. In our mouse model of polyglutamine disease (Q64 mice), clear decreases in H4 acetylation were also observed. Addition of butyrate, an inhibitor of HDAC, dramatically recovered or even enhanced the acetylated levels of histones H3 and H4 in PC12 cells, so that cells with or without expanded polyglutamine expression indistinguishable. These observations fit well with the idea that expanded polyglutamine tracts contribute to enhancement of histone deacetylation rather than to diminishment of histone acetylation.

Sequestration of major transcription factors such as CBP within polyglutamine aggregates has been proposed to be the main mechanism underlying transcriptional suppression in aggregate-containing cells (17, 44). Because these transcription factors, either by themselves or by physical interactions, contribute to HAT activation, this putative mechanism would lead to a diminishment of histone acetylation rather than to an enhancement of histone deacetylation, and was in direct contrast with our observations. Furthermore, irrespective of the intracellular localization of polyglutamine aggregates, we observed clear decreases in the acetylated levels of histones H3 and H4. More surprisingly, NES-tagged Q79 could induce stronger histone deacetylation than could NLS-tagged Q79. These observations strongly suggest the existence of a mechanism other than sequestration of transcription factors, in which expanded polyglutamine expression, even in the cytoplasm, leads to H3 and H4 deacetylation, probably via HDAC activation.

In cells expressing expanded polyglutamines, three sequential amino acids in VCP, Ser-612, Thr-613, and Lys-614, were modified by phosphorylation, phosphorylation, and acetylation, respectively. We then examined the biological significance of these modifications by creating and expressing several modification-mimic forms of VCPs, such as VCP(DEQ) and VCP(DEK), in PC12 cells. We also created several control substitutions with alanine, *e.g.* VCP(DEA) and VCP (AAA). Although these substitutions may not perfectly represent modified or non-modified protein configurations, this method has been well-used in elucidating biological functions of the modified or non-modified proteins, respectively, such as kinases, kinase substrates, tubulin, histones etc (45–47).

We found that in more than 95% of cells, exogenously expressed wtVCP stayed in the cytoplasm. In contrast, in more than 60% of transfected cells, exogenously expressed VCP-(DEQ) was translocated to the nucleus, followed by VCP-(DEA)(~50%) and VCP(DEK)(~25%). In accordance with this, FLAG-tagged VCP(DEQ), but not wtVCP, could co-precipitate endogenous importins (data not shown). These results strongly suggest that sequential modifications of Ser-612, Thr-613, and Lys-614 were responsible for the nuclear translocation of VCP. Unexpectedly, these modifications also induced neurite retraction and shrinkage in PC12 cells (~30% of cells), which was also observed in PC12 cells expressing expanded polyglutamine tracts. This atrophic phenotype was not induced by forced expression of NLS-tagged wtVCP in the nucleus or by forced expression of NES-tagged VCP(DEQ) in the cytoplasm. In agreement with these results, forced expression of NLS-tagged VCP(DEQ) in the nucleus further increased the atrophic phenotype in cells (~60% of cells).

The above characteristics of VCP suggest that it might be a mediator of histone deacetylation in response to expanded polyglutamines. Indeed, expression of VCP(DEQ), but not wtVCP or VCP(AAA), induced deacetylation of H3 and H4. More importantly, in mammalian cells NES-wtVCP and NES-VCP(AAA), but not VCP(AAA), inhibited the nuclear translocation of endogenous VCP in cells expressing expanded polyglutamines, and thus could block expanded polyglutamine-induced deacetylation of H3 and H4, as well as the atrophic phenotype. In *Drosophila*, however, wtVCP but not ter94 could prevent ter94 nuclear translocation in a way similar to NES-wtVCP or NES-VCP(AAA) in mammalian cells. Since VCP forms hexameric structure, the observed three sequential modifications of VCP in mammalian cells would not occur so frequently. However, once such modifications occur even in a single or double protomers, the VCP hexamer may be transported into the nucleus. Thus, VCP(AAA) could not suppress the nuclear translocation of the VCP hexamer. In *Drosophila* cells, however, the presence of the unmodified mammalian VCP in the ter94 hexamer did prevent the nuclear translocation of the hexamer even in the presence of polyglutamine aggregates. This might be due to the creation of certain conformations unfavorable for the nuclear translocation of the hexamer by the incorporation of unmodified mammalian VCP. This idea remains to be clarified. In contrast, expression of VCP(DEQ) itself in fly eyes induced eye degenerations, with decreased core histone acetylations. These results demonstrate that VCP is indeed a major mediator of histone deacetylation, as well as a major molecule causative for the atrophic phenotype or eye degenerations in cells expressing expanded polyglutamines. In our mouse model of polyglutamine disease (Q64C mouse), Purkinje cells with nuclear polyglutamine aggregates clearly showed nuclear VCP localization and decrease of acetylation of histone H4. Recently, Reina *et al.* demonstrated that MJD protein/ataxin 3 translocated into the nucleus immediately after the heat shock. In this condition, VCP appeared to stay in the cytoplasm (48). It would also be interesting to see whether histone deacetylation could be observed after the heat shock.

Until now, at least 14 different VCP mutants have been reported to cause IBMPFD. The mutated amino acids include R93C, R95C R95G, R155C, R155H, R155P, G157R, R159H, R159C, R191Q, L198W, A232E, T262A, and N387H (35–39).

FIGURE 7. **Ameliorative effects of wtVCP on polyglutamine-induced eye degeneration and deacetylation of core histones in *Drosophila* eyes.** *A*, light photomicrographs of the compound eyes from 5-day-old flies. Wild-type VCP (*wtVCP*) was expressed alone or together with FLAG-Q92 (*Q92*) in *Drosophila* compound eyes using the GMR promoter. *Bar*, 100 μm. *B–D*, immunohistochemical analysis of tangential head sections from 5-day-old flies. Q92 was detected with an anti-FLAG M5 antibody, acetyl-H3 with an anti-acetylated histone H3 antibody, and VCP/ter94 with an anti-VCP polyclonal antibody. Each section was co-stained with TOTO-3. Merged images are also shown in the *lower panels* with indicated colors. Cells with ter94 dominantly residing in the nucleus are indicated by *red arrows* and with VCP/ter94 dominantly residing outside the nucleus indicated by *red arrowheads* (*C*). *Bars*, 20 μm (*B* and *D*) and 10 μm (*C*). *E*, quantification of immunohistochemical analysis in *D*. More than 200 cells were examined in each sample, and the ratio of nuclei with acetylated histone H3 among TOTO-3-positive nuclei in the retina were counted. **, $p < 0.01$; *, $p < 0.05$.

Except for Thr-262, all other mutations were not observed at serine, threonine, tyrosine, or lysine. Since alanine substitution cannot mimick phosphorylation, all these mutations are not able to be mimicked by post-translational modifications, such as phosphorylations or acetylations. It is notable that all mutations relatively reside at N-terminal portion of VCP. Indeed, these mutant VCPs not only showed enhanced binding abilities to VCP cofactors (*e.g.* Ufd1 and Npl4) and ubiquitinated proteins, but also showed enhanced aggregate-forming activities (Refs. 28, 49).[3] Regarding with these characteristics, we could not observe clear difference between wild-type VCP and VCP(DEQ).[4] Thus, VCP(DEQ) did not appear to be involved in aggregate formation more positively than wild-type VCP or IBMPFD-causing VCPs.

Treatment of cells expressing expanded polyglutamine or VCP(DEQ) by butyrate did result in a recovery from the H3 and H4 deacetylated state to highly acetylated states. However, this treatment only marginally increased transcription from the CMV promoter and several other promoters, such as the EF-1α promoter. These results clearly indicate that the observed transcriptional suppression was mostly mediated by as-yet unknown HDAC inhibitor-insensitive mechanisms.

Based on the results of this study, we propose a novel feedback mechanism linking the accumulation of cytoplasmic misfolded proteins and transcriptional suppression, in which VCP performs an essential role. Intracellular accumulation of abnormal proteins such as expanded polyglutamines induces VCP modification at Ser-612, Thr-613, and Lys-614, which allows VCP to translocate to the nucleus. Following nuclear VCP translocation, general transcription is suppressed by as-yet unknown mechanisms, resulting in the inhibition of *de novo* protein synthesis. This inhibition leads to a decrease in the production of new misfolded proteins, and thus allows to cells to dissolve or degrade the accumulated misfolded proteins by cellular mechanisms such as chaperones, proteasomes, and autophagies. This mechanism would work well when misfolded protein accumulation is transient. However, when misfolded proteins are continuously provided, as in the case of neurodegenerative disorders, inhibition of *de novo* protein synthesis continues for many years or even decades, leading to a gradual decrease in cell mass or shrinkage of affected neurons. Indeed, overexpression of VCP(DEQ) in fly eyes could induce late-onset rough-eye phenotypes. This VCP-mediated feedback mechanism may be a common mechanism underlying neurodegenerative disorders in which there is an intracellular accumulation of abnormal proteins such as polyglutamines, α-synuclein etc.

Acknowledgments—We thank K. Kuroiwa for technical assistance and our laboratory members for valuable discussions. We also thank Drs. T. Kanda and S. Mori (Japan National Institute of Infectious Disease) for pHrD-Luc.

REFERENCES

1. Kaufman, R. J. (2002) *J. Clin. Invest.* **110,** 1389–1398
2. Sidrauski, C., Chapman, R., and Walter, P. (1998) *Trends Cell Biol.* **8,** 245–249
3. Ron, D., and Walter, P. (2007) *Nat. Rev. Mol. Cell Biol.* **8,** 519–529
4. Kakizuka, A. (1998) *Trends Genet.* **14,** 396–402
5. Kobayashi, T., and Kakizuka, A. (2003) *Cytogenet. Genome Res.* **100,** 261–275
6. Neumann, M., Sampathu, D. M., Kwong, L. K., Truax, A. C., Micsenyi, M. C., Chou, T. T., Bruce, J., Schuck, T., Grossman, M., Clark, C. M., McCluskey, L. F., Miller, B. L., Masliah, E., Mackenzie, I. R., Feldman, H., Feiden, W., Kretzschmar, H. A., Trojanowski, J. Q., and Lee, V. M. (2006) *Science* **314,** 130–133
7. Ikeda, H., Yamaguchi, M., Sugai, S., Aze, Y., Narumiya, S., and Kakizuka, A. (1996) *Nat. Genet.* **13,** 196–202
8. Bence, N. F., Sampat, R. M., and Kopito, R. R. (2001) *Science* **292,** 1552–1555
9. Nishitoh, H., Matsuzawa, A., Tobiume, K., Saegusa, K., Takeda, K., Inoue, K., Hori, S., Kakizuka, A., and Ichijo, H. (2002) *Genes Dev.* **16,** 1345–1355
10. Ross, C. A., and Pickart, C. M. (2004) *Trends Cell Biol.* **14,** 703–711
11. Giuliano, P., DeCristofaro, T., Affaitati, A., Pizzulo, G. M., Feliciello, A., Criscuolo, C., DeMichele, G., Filla, A., Avvedimento, E. V., and Varrone, S. (2003) *Hum. Mol. Genet.* **12,** 2301–2309
12. Shimohata, T., Nakajima, T., Yamada, M., Uchida, C., Onodera, O., Naruse, S., Kimura, T., Koide, R., Nozaki, K., Sano, Y., Ishiguro, H., Sakoe, K., Ooshima, T., Sato, A., Ikeuchi, T., Oyake, M., Sato, T., Aoyagi, Y., Hozumi, I., Nagatsu, T., Takiyama, Y., Nishizawa, M., Goto, J., Kanazawa, I., Davidson, I., Tanese, N., Takahashi, H., and Tsuji, S. (2000) *Nat. Genet.* **26,** 29–36
13. Steffan, J. S., Bodai, L., Pallos, J., Poelman, M., McCampbell, A., Apostol, B. L., Kazantsev, A., Schmidt, E., Zhu, Y. Z., Greenwald, M., Kurokawa, R., Housman, D. E., Jackson, G. R., Marsh, J. L., and Thompson, L. M. (2001) *Nature* **413,** 739–743
14. Hassig, C. A., and Schreiber, S. L. (1997) *Curr. Opin. Chem. Biol.* **1,** 300–308
15. Shilatifard, A. (2006) *Annu. Rev. Biochem.* **75,** 243–269
16. Saha, R. N., and Pahan, K. (2006) *Cell Death Differ.* **13,** 539–550
17. Nucifora, F. C., Jr., Sasaki, M., Peters, M. F., Huang, H., Cooper, J. K., Yamada, M., Takahashi, H., Tsuji, S., Troncoso, J., Dawson, V. L., Dawson, T. M., and Ross, C. A. (2001) *Science* **291,** 2423–2428
18. Yu, Z. X., Li, S. H., Nguyen, H. P., and Li, X. J. (2002) *Hum. Mol. Genet.* **11,** 905–914
19. Jiang, H., Nucifora, F. C., Jr., Ross, C. A., and DeFranco, D. B. (2003) *Hum. Mol. Genet.* **12,** 1–12
20. Rouaux, C., Jokic, N., Mbebi, C., Boutillier, S., Loeffler, J. P., and Boutillier, A. L. (2003) *EMBO J.* **22,** 6537–6549
21. Kontopoulos, E., Parvin, J. D., and Feany, M. B. (2006) *Hum. Mol. Genet.* **15,** 3012–3023
22. Rouaux, C., Panteleeva, I., René, F., Gonzalez de Aguilar, J. L., Echaniz-Laguna, A., Dupuis, L., Menger, Y., Boutillier, A. L., and Loeffler, J. P. (2007) *J. Neurosci.* **27,** 5535–5545
23. Whiteheart, S. W., and Matveeva, E. A. (2004) *J. Struct. Biol.* **146,** 32–43
24. Braun, R. J., and Zischka, H. (2008) *Biochim. Biophys. Acta* **1783,** 1418–1435
25. Hirabayashi, M., Inoue, K., Tanaka, K., Nakadate, K., Ohsawa, Y., Kamei, Y., Popiel, A. H., Sinohara, A., Iwamatsu, A., Kimura, Y., Uchiyama, Y., Hori, S., and Kakizuka, A. (2001) *Cell Death Differ.* **8,** 977–984
26. Mizuno, Y., Hori, S., Kakizuka, A., and Okamoto, K. (2003) *Neurosci. Lett.* **343,** 77–80
27. Ishigaki, S., Hishikawa, N., Niwa, J., Iemura, S., Natsume, T., Hori, S., Kakizuka, A., Tanaka, K., and Sobue, G. (2004) *J. Biol. Chem.* **279,** 51376–51385
28. Kakizuka, A. (2008) *Biochem. Soc. Trans.* **36,** 105–108
29. Kobayashi, T., Manno, A., and Kakizuka, A. (2007) *Genes Cells* **12,** 889–901
30. Higashiyama, H., Hirose, F., Yamaguchi, M., Inoue, Y. H., Fujikake, N., Matsukage, A., and Kakizuka, A. (2002) *Cell Death Differ.* **9,** 264–273
31. Klein, J. B., Barati, M. T., Wu, R., Gozal, D., Sachleben, L. R., Jr., Kausar, H., Trent, J. O., Gozal, E., and Rane, M. J. (2005) *J. Biol. Chem.* **280,** 31870–31881
32. Livingstone, M., Ruan, H., Weiner, J., Clauser, K. R., Strack, P., Jin, S.,

[3] A. Manno and A. Kakizuka, unpublished observations.
[4] K. Yasuda and A. Kakizuka, unpublished observations.

Williams, A., Greulich, H., Gardner, J., Venere, M., Mochan, T. A., DiTullio, R. A., Jr., Moravcevic, K., Gorgoulis, V. G., Burkhardt, A., and Halazonetis, T. D. (2005) *Cancer Res.* **65,** 7533–7540
33. Noguchi, M., Takata, T., Kimura, Y., Manno, A., Murakami, K., Koike, M., Ohizumi, H., Hori, S., and Kakizuka, A. (2005) *J. Biol. Chem.* **280,** 41332–41341
34. Mori-Konya, C., Kato, N., Maeda, R., Yasuda, K., Higashimae, N., Noguchi, M., Koike, M., Kimura, Y., Ohizumi, H., Hori, S., and Kakizuka, A. (2009) *Genes Cells* **14,** 483–497
35. Watts, G. D., Wymer, J., Kovach, M. J., Mehta, S. G., Mumm, S., Darvish, D., Pestronk, A., Whyte, M. P., and Kimonis, V. E. (2004) *Nat. Genet.* **36,** 377–381
36. Haubenberger, D., Bittner, R. E., Rauch-Shorny, S., Zimprich, F., Mannhalter, C., Wagner, L., Mineva, I., Vass, K., Auff, E., and Zimprich, A. (2005) *Neurology* **65,** 1304–1305
37. Forman, M. S., Mackenzie, I. R., Cairns, N. J., Swanson, E., Boyer, P. J., Drachman, D. A., Jhaveri, B. S., Karlawish, J. H., Pestronk, A., Smith, T. W., Tu, P. H., Watts, G. D., Markesbery, W. R., Smith, C. D., and Kimonis, V. E. (2006) *J. Neuropathol. Exp. Neurol.* **65,** 571–581
38. Kimonis, V. E., Fulchiero, E., Vesa, J., and Watts, G. (2008) *Biochim. Biophys. Acta* **1782,** 744–748
39. Djamshidian, A., Schaefer, J., Haubenberger, D., Stogmann, E., Zimprich, F., Auff, E., and Zimprich, A. (2009) *Muscle Nerve* **39,** 389–391
40. Yasuda, S., Inoue, K., Hirabayashi, M., Higashiyama, H., Yamamoto, Y., Fuyuhiro, H., Komure, O., Tanaka, F., Sobue, G., Tsuchiya, K., Hamada, K., Sasaki, H., Takeda, K., Ichijo, H., and Kakizuka, A. (1999) *Genes Cells* **4,** 743–756
41. Yanagawa, S., Lee, J. S., and Ishimoto, A. (1998) *J. Biol. Chem.* **273,** 32353–32359
42. Mori, S., Ozaki, S., Yasugi, T., Yoshikawa, H., Taketani, Y., and Kanda, T. (2006) *Mol. Cell. Biochem.* **288,** 47–57
43. Kobayashi, T., Tanaka, K., Inoue, K., and Kakizuka, A. (2002) *J. Biol. Chem.* **277,** 47358–47365
44. Schaffar, G., Breuer, P., Boteva, R., Behrends, C., Tzvetkov, N., Strippel, N., Sakahira, H., Siegers, K., Hayer-Hartl, M., and Hartl, F. U. (2004) *Mol. Cell* **15,** 95–105
45. Holmberg, C. I., Tran, S. E., Eriksson, J. E., and Sistonen, L. (2002) *Trends Biochem. Sci.* **27,** 619–627
46. Gaertig, J., and Wloga, D. (2008) *Curr. Top. Dev. Biol.* **85,** 83–113
47. Edmondson, D. G., Davie, J. K., Zhou, J., Mirnikjoo, B., Tatchell, K., and Dent, S. Y. (2002) *J. Biol. Chem.* **277,** 29496–29502
48. Reina, C. P., Zhong, X., and Pittman, R. N. (2010) *Hum. Mol. Genet.* **19,** 235–249
49. Ju, J. S., Miller, S. E., Hanson, P. I., and Weihl, C. C. (2008) *J. Biol. Chem.* **283,** 30289–30299
50. Trottier, Y., Luts, Y., Stevanin, G., Imbert, G., Devys, D., Cancel, G., Saudou, F., Weber, C., David, G., Tora, L., Agid, Y., Brice, A., and Mandel, J. L. (1995) *Nature* **378,** 403–406

Genes to Cells

Enhanced ATPase activities as a primary defect of mutant valosin-containing proteins that cause inclusion body myopathy associated with Paget disease of bone and frontotemporal dementia

Atsushi Manno[1,2], Masakatsu Noguchi[1,2], Junpei Fukushi[1,2], Yasuhiro Motohashi[1,2] and Akira Kakizuka[1,2]*

[1]*Laboratory of Functional Biology, Kyoto University Graduate School of Biostudies, Kyoto 606-8501, Japan*
[2]*SORST, Japan Science and Technology Agency*

Valosin-containing protein (VCP) has been shown to colocalize with abnormal protein aggregates, such as nuclear inclusions of Huntington disease and Machado-Joseph disease, Lewy bodies in Parkinson disease. Several mis-sense mutations in the human *VCP* gene have been identified in patients suffering inclusion body myopathy associated with Paget disease of bone and frontotemporal dementia (IBMPFD). Recently, we have shown that VCP possesses both aggregate-forming and aggregate-clearing activities. Here, we showed that in cells treated with proteasome inhibitors VCP first appeared as several small aggregates throughout the cells; and then, these small aggregates gathered together into a single big aggregate. Subcellular localization and ATPase activity of VCP clearly influenced the localization of the aggregates. Furthermore, all tested IBMPFD-causing mutant VCPs, possessed elevated ATPase activities and enhanced aggregate-forming activities in cultured cells. In *Drosophila*, these mutants and VCP(T761E), a super active VCP, did not appear to spontaneously induce eye degeneration, but worsened the phenotype when co-expressed with polyglutamines. Unexpectedly, these VCPs did not apparently change sizes and the amounts of polyglutamine aggregates in *Drosophila* eyes. Elevated ATPase activities, thus, may be a hidden primary defect causing IBMPFD pathological phenotypes, which would be revealed when abnormal proteins are accumulated, as typically observed in aging.

Introduction

VCP belongs to the AAA (ATPase associated with diverse cellular activities) proteins, forms a homohexameric structure and consists of the N-terminal domain (N domain), two ATPase domains (D1 and D2 domains) and the C-terminal domain (Zhang *et al.* 2000; Dalal & Hanson 2001; Brunger & DeLaBarre 2003; Wang *et al.* 2004). VCP is one of the most abundant and ubiquitous intracellular proteins (Dalal & Hanson 2001). It has been shown that VCP is involved in diverse cellular activities, including proteasome-mediated protein degradation, endoplasmic reticulum (ER)-associated degradation (ERAD), membrane fusions and mitosis (Wang *et al.* 2004). In performing different functions, VCP has been proposed to differentially use its partners, e.g. Ufd1, Npl4, p47 (Dreveny *et al.* 2004). VCP has been also shown to be modified at many amino acid residues throughout the protein via oxidation, phosphorylation and acetylation (Noguchi *et al.* 2005; Mori-Konya *et al.* 2009; Koike *et al.* 2010). Previously, we have identified VCP as a binding partner of the Machado-Joseph disease (MJD) protein with expanded polyglutamines, which causes MJD, the most common inherited spinocerebellar ataxia (Kawaguchi *et al.* 1994; Hirabayashi *et al.* 2001). We have also identified *ter94*, *Drosophila* homologue of VCP, as a modifier of expanded polyglutamine-induced eye degeneration by genetic screening using our *Drosophila* polyglutamine disease models (Higashiyama *et al.* 2002). Interestingly,

Communicated by: Eisuke Nishida
**Correspondence*: kakizuka@lif.kyoto-u.ac.jp

DOI: 10.1111/j.1365-2443.2010.01428.x

we have shown that VCP colocalized with abnormal protein aggregates or ubiquitin-positive inclusion bodies in neurons suffering from several neurodegenerative disorders including not only MJD but also Huntington disease, Parkinson disease, motor neuron disease and so on (Hirabayashi *et al.* 2001; Mizuno *et al.* 2003; Ishigaki *et al.* 2004). Under the proteasome inhibition and/or the accumulation of ubiquitin-positive proteins, small aggregates are first formed in the cytoplasm, and then they are transported to the microtubule organizing center near the nucleus (Johnston *et al.* 1998; García-Mata *et al.* 1999). The resultant ubiquitin-positive structure is called the aggresome (Johnston *et al.* 1998). The transport has been proposed to occur along the microtubules by dynein/dynactin motor proteins and HDAC6 (Johnston *et al.* 2002; Kawaguchi *et al.* 2003). The aggresome is also surrounded by vimentin, an intermediate filament protein, and thus ubiquitin and vimentin stainings are well used to elucidate the position of aggresome in histochemical studies. VCP immunostaining was also observed in aggresomes induced by proteasome inhibition and in polyglutamine aggregates in cells expressing expanded polyglutamines (Hirabayashi *et al.* 2001). However, the significance of such colocalization remains to be elucidated. Recently, we have demonstrated that VCP is involved in the formation and/or clearance of abnormal protein aggregates and that it is also involved in the re-solubilization and re-activation of heat-denatured proteins from insoluble aggregates (Kobayashi *et al.* 2007). Hence, we have proposed that VCP functions not only as an aggregate-formase but also as an aggregate-unfoldase (Kobayashi *et al.* 2007).

Inclusion body myopathy associated with Paget disease of bone and frontotemporal dementia (IBMPFD) is a rare, complex, late-onset and ultimately lethal disorder with the autosomal dominant inheritance (OMIM 605382) (Kimonis *et al.* 2000; Watts *et al.* 2004). The most common manifestation is adult-onset muscle weakness with myopathy (80–90% of affected individuals). Paget disease of bone (PDB) and frontotemporal dementia (FTD) occur less frequently than muscle myopathy (43–57%; PDB, 27–37%; FTD) (Kimonis *et al.* 2000, 2008; Kovach *et al.* 2001; Kimonis & Watts 2005). Several groups have reported that 7 mis-sense mutations in the gene encoding VCP were identified among the patients with IBMPFD (277C → T, 283C → G, 463C → T, 464G → A, 464G → C, 476G → A, 572G → A and 695C → A, resulting in the amino acid substitutions R93C, R95G, R155C, R155H, R155P, R159H, R191Q and A232E) (Watts *et al.* 2004; Haubenberger *et al.* 2005; Hübbers *et al.* 2007). Furthermore, novel mutations in VCP (R95C, G157R, R159C, L198W, T262A and N387H) have also been reported (Forman *et al.* 2006; Watts *et al.* 2007; Djamshidian *et al.* 2009; Weihl *et al.* 2009). Among 10 amino acid residues mutated in IBMPFD, 7 are conserved between *Drosophila* and human beings (R155, R159, R191, L198, A232, T262 and N387 are conserved, but not R93, R95 or G157) (Mori-Konya *et al.* 2009). It is notable that Arg93 is changed to Cys in *Drosophila*. In skeletal muscles and in neurons of the central nervous system of patients with IBMPFD, VCP-positive aggregates or VCP-rimmed vacuoles were observed (Watts *et al.* 2004; Schröder *et al.* 2005). Recently, it has been reported that IBMPFD-associated VCP mutants disrupt ERAD (Weihl *et al.* 2006), impair aggresome formation (Ju *et al.* 2008) as well as autophagy (Ju *et al.* 2009). However, pathogenic mechanisms underlying IBMPFD are still controversial and remain unclear.

In this study, we demonstrate that all tested IBMPFD-associated VCP mutants possess elevated ATPase activities as well as enhanced aggregate-forming activities together with cofactor-binding abilities especially on Ufd1 and Npl4 in mammalian cells, which apparently enhances their binding abilities to ubiquitinated proteins. Furthermore, VCP mutants of higher ATPase activities worsened the phenotypes when co-expressed with polyglutamines in *Drosophila* eyes, even without apparently affecting aggregates. These observations suggest that constitutively elevated ATPase activities of VCP are primary abnormalities causing IBMPFD.

Results

VCP in abnormal protein aggregate formation

In order to define the way as to how VCP involves in protein aggregate formation, we transfected HEK293 cells with expression vectors for VCP-GFP and FLAG-Q35 (Q35) or -Q79 (Q79), which encodes FLAG-tagged 35 or 79 repeats of glutamine residues, respectively, and examined their colocalization. One day after transfection, we found that VCP-GFP colocalized with small Q79 aggregates, which appeared as several dots throughout the cells (Fig. 1A, middle panels). Two days after transfection, most cells had one big aggregate, and this aggregate was labeled with GFP signals (Fig. 1A, lower panels). To examine the entire processes more precisely, we traced GFP

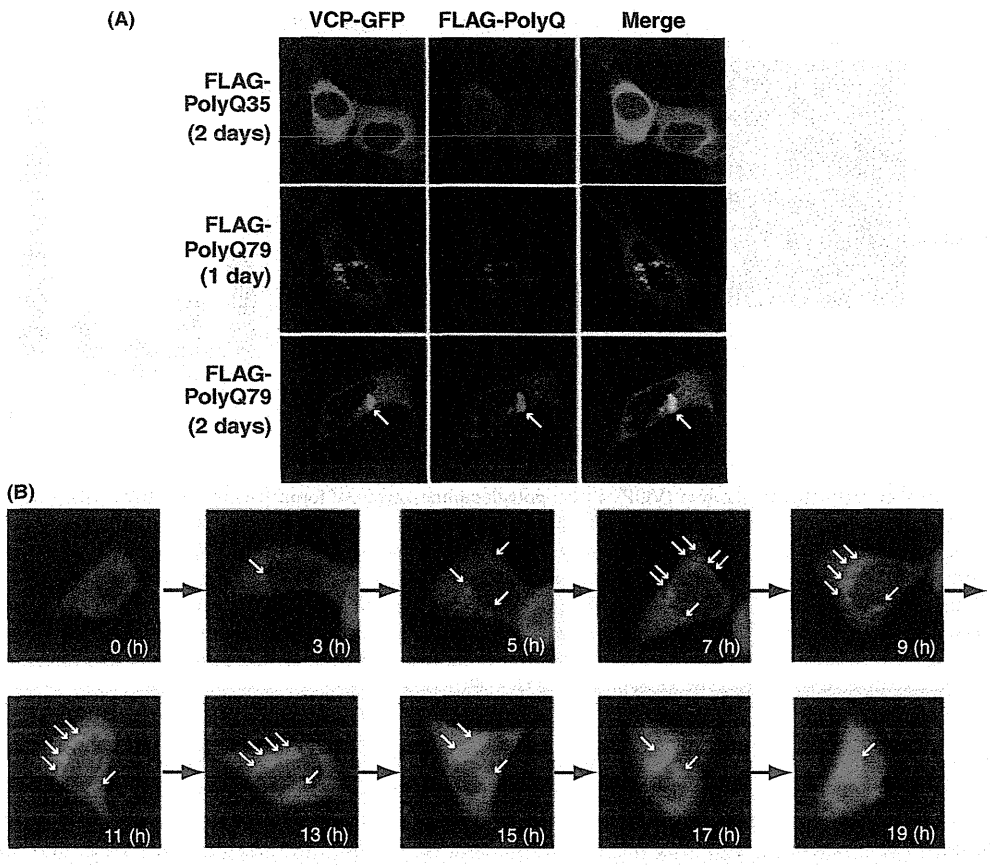

Figure 1 Localization of valosin-containing protein (VCP) in protein aggregates in cultured cells. (A) Localization of VCP and polyglutamine aggregates in HEK293 cells co-expressing VCP-GFP and FLAG-Q35 or -Q79 for 1 or 2 days. VCP (green signals), and Q35 or Q79 (red signals) were visualized via fluorescence microscopy. (B) After expression of VCP-GFP and treatment with 1 μM MG132 (time 0 h), HEK293 cells were examined under time-lapse fluorescence microscopy. Several small protein aggregates were observed in the cytoplasm after 3–7 h; and then, these small aggregates were gathered to a single large aggregate after 9–19 h. White arrows indicate positions of aggregates (A) and (B).

signals in a HEK293 cell expressing VCP-GFP after treatment with MG132 (a proteasome inhibitor), which is known to create the aggresome in the cytoplasm (Johnston *et al.* 1998). Before treatment with MG132, VCP-GFP was distributed diffusely throughout the cytoplasm in the cell, but approximately 3–6 h after the treatment, GFP signals appeared as small dots in several different portions of the cell. Then, after 9–19 h, these GFP-positive small aggregates moved to a single big aggregate, which is generally called an aggresome (Johnston *et al.* 1998) (Fig. 1B, Video S1 in Supplementary materials.).

These results suggested that VCP may function as a carrier of abnormal proteins for collecting them into the aggresome. If so, VCP localization may affect the localizations of protein aggregates. In order to test this, we expressed Q79 together with VCP-GFP, NES-VCP-GFP or NLS-VCP-GFP in HEK293 cells and examined the localizations of the aggregates. Among the GFP-positive cells, less than 10% of the cells contained Q79 aggregates in the nucleus in HEK293 cells expressing VCP-GFP or NES-VCP-GFP, in which GFP signals were observed mostly in the cytoplasm (Fig. 2A,B). On the other hand, nearly 50% of cells contained Q79 aggregates in the nucleus of HEK293 cells expressing NLS-VCP-GFP, where GFP signals were observed mostly in the nucleus (Fig. 2A,B). Interestingly, when we expressed NLS-tagged VCP(K524A), an ATPase activity-deficient VCP mutant (Hirabayashi *et al.* 2001; Kobayashi *et al.*

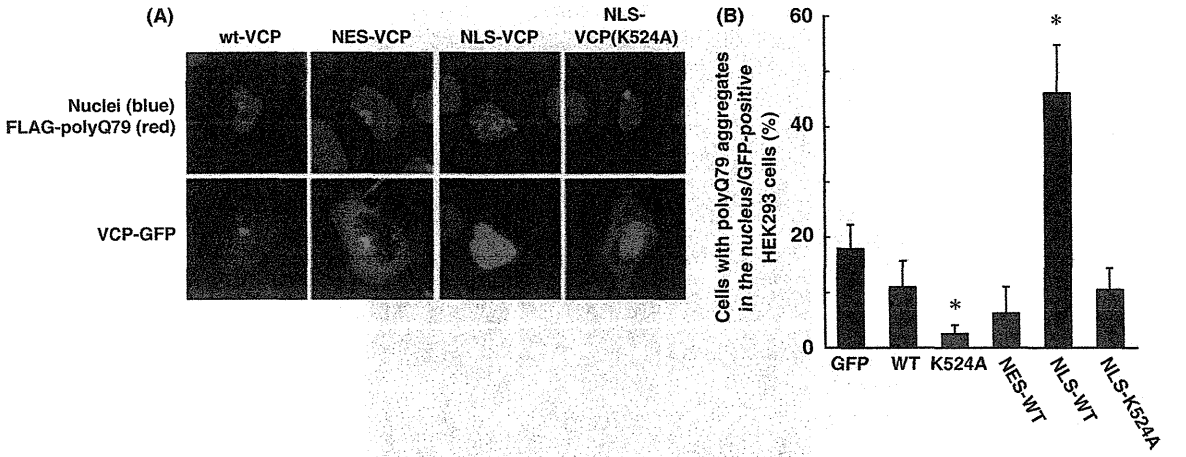

Figure 2 Effects of valosin-containing protein (VCP) on the polyglutamine aggregate formation. (A) HEK293 cells were transfected with wt-VCP-GFP, NES-wt-VCP-GFP, NLS-wt-VCP-GFP or NLS-VCP(K524A)-GFP, together with FLAG-Q79. Two days after transfection, cells were processed for immunochemical analysis. VCP (green signals), Q79 (red signals) and nuclei (blue signals) were visualized via fluorescence microscopy. Note that in cells expressing NES-VCP, a big single polyQ aggregate was observed in microtubule organizing center near the nucleus. (B) The numbers of cells with polyglutamine aggregates in the nucleus and GFP-positive cells were counted in five different fields in the condition described in (A), and percentages of cells with polyglutamine aggregates in the nucleus among GFP-positive cells are shown. Mean values of five independent fields are indicated. Error bars represent standard deviations. Statistical analysis was performed by Student's *t*-test (*$P < 0.01$ vs. WT).

2002), Q79 aggregates were observed mostly in the cytoplasm but not in the nucleus in the cells (Fig. 2A,B), although the aggregates were less frequently formed. These results suggest that the VCP is able to transport abnormal proteins, probably functioning as a carrier, and that its ATPase activities are necessary for this performance.

Involvement of VCP cofactors in aggregate formation

We then investigated the role of VCP cofactors on abnormal protein aggregate formation using the RNAi technique. We examined the efficiency of various siRNAs on the polyglutamine aggregate formation in HEK293 cells (Fig. 3). In Western blotting, we observed that VCP siRNA decreased expression levels of not only VCP but also Npl4 and Ufd1 (Fig. 3A). p47 siRNA specifically reduced p47 expression levels (Fig. 3A), whereas Npl4 siRNA almost completely depleted expression levels of both Npl4 and Ufd1 (Fig. 3A). Likewise, Ufd1 siRNA induced a strong depletion of Ufd1 as well as a weak depletion of Npl4 (Fig. 3A). Previously, it has been reported that Npl4 siRNA decreased Ufd1 protein levels and that Ufd1 siRNA or Npl4 siRNA decreased VCP-Ufd1-Npl4 complex by approximately 90% (Nowis *et al.* 2006). These data and our data did not match perfectly, but as a whole, suggest that protein levels of VCP, Npl4 and Ufd1 were affected by each other. We observed that not only the decrease in VCP, but also the decrease in Npl4 and Ufd1 inhibited Q79 aggregate formation by immunochemical analysis in HEK293 cells (Fig. 3B,C). In contrast, decrease in p47 did not apparently affect the aggregate formation (Fig. 3B,C).

Enhancement of aggregate-forming and ATPase activities in IBMPFD-VCPs

Recently, we have proposed that VCP functions as both an aggregate-formase and aggregate-unfoldase (Kobayashi *et al.* 2007). The results earlier suggested that VCP functions as a carrier of abnormal proteins into aggregates. These results led to the possibility that IBMPFD-causing VCP mutants cause the acceleration of abnormal protein aggregate formation. To address this possibility, we examined the effects of the expression of IBMPFD-causing VCP mutants (IBMPFD-VCPs) on forming abnormal protein aggregates induced by proteasome inhibition or expanded polyglutamine expression. By treatment with proteasome inhibitors, we found significant increase in cell populations having aggregated GFP signals by expressing all tested GFP-tagged IBMPFD-

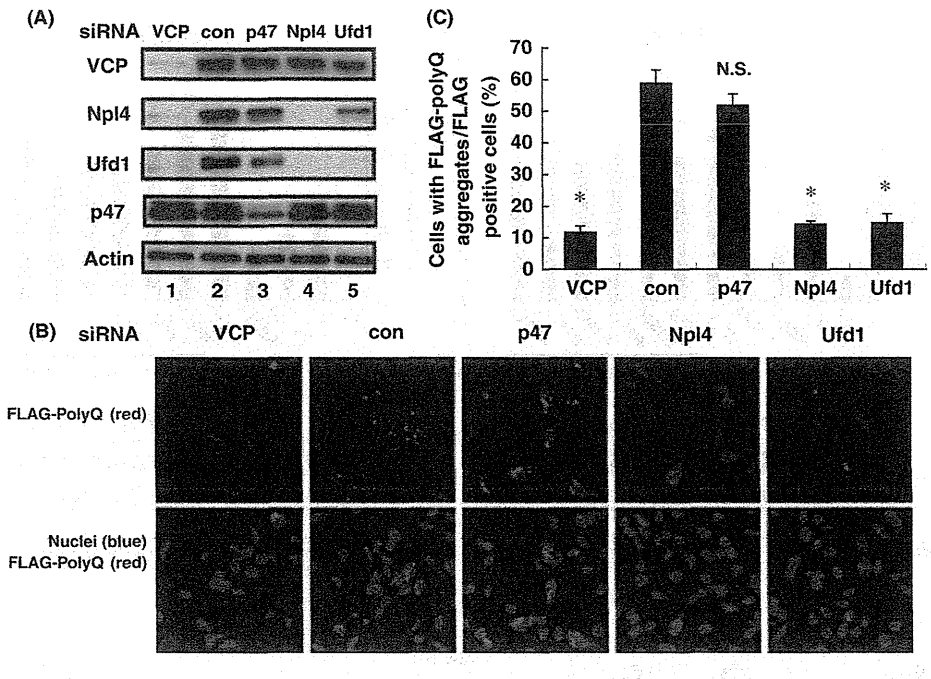

Figure 3 Effects of valosin-containing protein (VCP) cofactors on the polyglutamine aggregate formation. (A) Effects of VCP cofactors depletion by siRNA in HEK293 cells. HEK293 cells were transfected with VCP siRNA (ncds), control siRNA, p47 siRNA (1477), Npl4 siRNA (679) and Ufd1 siRNA (216). Expression levels of VCP, Npl4, Ufd1, p47 and actin, as a loading control, were detected by Western blot analysis. (B) Formation of polyglutamine aggregates in cells expressing both FLAG-Q79 and VCP siRNA (ncds), control siRNA, p47 siRNA (1477), Npl4 siRNA (679) and Ufd1 siRNA (216). The cells described in (A) were visualized by fluorescence microscopy, and Q79 (red signals) and the nucleus (blue signals) were visualized. (C) Effects of the knockdown of VCP cofactors on the polyglutamine aggregate formation. The numbers of cells with polyglutamine aggregates and FLAG-positive cells were counted in five different fields in condition described in (A), and the percentages of cells with polyglutamine aggregates among FLAG-positive cells are shown. Mean values of five independent fields are indicated. Error bars represent standard deviations. Statistical analysis was performed by Student's *t*-test (*$P < 0.01$; N.S., not significant vs. control siRNA).

VCPs when compared to expressing GFP-tagged wt-VCP (Fig. 4A). We also transfected HEK293 cells with GFP-tagged VCP(K524A) or VCP(K251A), ATPase activity-deficient VCP mutants (Hirabayashi *et al.* 2001; Kobayashi *et al.* 2002). By adding proteasome inhibitors on cells expressing VCP(K251A)-GFP or VCP(K524A)-GFP, cell populations having aggregated GFP signals were significantly decreased when compared with cells expressing wt-VCP (Fig. 4A). Regarding with polyglutamine aggregates, we also observed significant increases in cell populations with aggregated GFP signals in cells expressing most of IBMPFD-VCPs and significant decreases in cells expressing ATPase activity-deficient mutants (Fig. 4B). Collectively, these data provided the evidence that formation of abnormal protein aggregates is enhanced in cells expressing IBMPFD-VCPs when compared with wt-VCP, as similar results have been published (Weihl *et al.* 2006).

We also noticed that enhancement of abnormal protein aggregate formation in cells expressing VCP(T761E), a super active VCP in HEK293 cells (Fig. 4A,B), which has more than twice as strong ATPase activity than wt-VCP (Mori-Konya *et al.* 2009). From these results, we hypothesized that ATPase activities of IBMPFD-VCPs would be higher than that of wt-VCP. We thus measured their ATPase activities and found that all tested IBMPFD-VCPs showed significantly higher ATPase activities, when compared with that of wt-VCP in two different assays (Fig. 4C,D).

We next investigated the binding abilities of IBMPFD-VCPs to VCP cofactors. We transfected HEK293 cells with FLAG-tagged wt-VCP, VCP

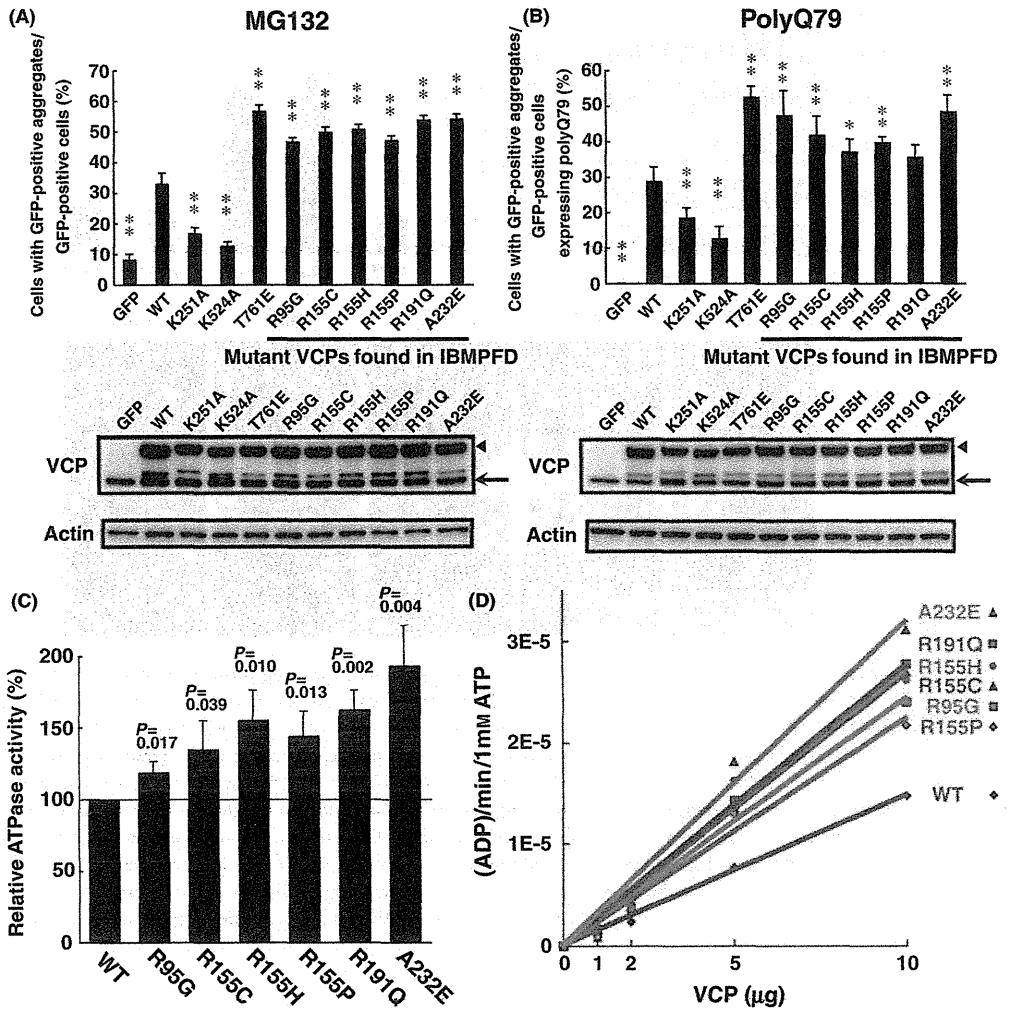

Figure 4 Enhanced aggregate-forming activities and ATPase activities in IBMPFD-VCPs. (A) Enhanced activities for MG132-induced aggregate formation in IBMPFD-VCPs. HEK293 cells were transfected with an expression plasmid for GFP or GFP-tagged VCPs. Twelve hours after transfection, cells were treated with 0.3 μM MG132 for 24 h. The number of cells with GFP-positive aggregates and GFP-positive cells was counted in five different fields. The percentages of cells with aggregates among GFP-positive cells are shown in the upper graph. Expression levels of various VCP-GFPs (VCP) and actin (actin) as a loading control are indicated in the lower panels. Arrowhead indicates bands of VCP-GFP, and arrow indicates bands of endogenous VCP. (B) Enhanced activities for polyglutamine aggregate formation in IBMPFD-VCPs. HEK293 cells were transfected with both an expression plasmid for GFP or GFP-tagged VCPs and an expression plasmid for FLAG-Q79. One day after transfection, the numbers of cells with GFP-positive aggregates and GFP-positive cells expressing FLAG-Q79 were counted in five different fields. The percentages of cells with GFP-positive aggregates among GFP-positive cells expressing FLAG-Q79 are shown in the upper graph. Expression levels of various VCP-GFPs (VCP) and actin (actin) as a loading control are indicated in the lower panels. Arrowhead indicates bands of VCP-GFP, and arrow indicates bands of endogenous VCP. Mean values of five independent fields are indicated. The error bars represent standard deviations. Statistical significance was calculated by Tukey's test (**$P < 0.01$, *$P < 0.05$ vs. WT, $n = 5$) (A) and (B). (C) and (D) Up-regulation of ATPase activities in IBMPFD-VCPs. ATPase activities of recombinant VCPs purified by HEK293 free style cells were compared. Their ATPase activities were measured using both the molybdate assay (C) and the NADH-coupled assay (D). See Experimental procedures in detail. Mean values of triplicate experiments are shown. Error bars represent standard deviations. *P*-values analyzed by Student's *t*-test are shown above the columns (C). IBMPFD, inclusion body myopathy associated with Paget disease of bone and frontotemporal dementia; VCP, valosin-containing protein.

(T761E) or IBMPFD-VCPs and immunoprecipitated FLAG-tagged VCPs with anti-FLAG M2 affinity gel. Coprecipitated endogenous Npl4, Ufd1, p47 and ubiquitinated proteins were examined by Western blot analysis. Npl4 and Ufd1 were coprecipitated more potently with all tested IBMPFD-VCPs than with wt-VCP (Fig. 5A). In contrast, the amounts of p47 precipitated with all IBMPFD-VCPs were only marginally higher than those precipitated with wt-VCP (Fig. 5A). Furthermore, polyubiquitinated proteins were more robustly bound to all tested IBMPFD-VCPs when compared with wt-VCP (Fig. 5A). These results suggest that the binding abilities to these cofactors, especially to Npl4 and Ufd1, were elevated in IBMPFD-VCPs. In contrast, wt-VCP and VCP(T761E) behave indistinguishably (Fig. 5B), indicating that the cofactor-binding abilities do not directly link to the ATPase activities. Knockdown of Npl4 and Ufd1 reduced the amount of coprecipitated polyubiquitinated proteins by IBMPFD-VCPs, as in VCP(R155C) and VCP(A232E) (Fig. 5C). These results suggest that binding of polyubiquitinated

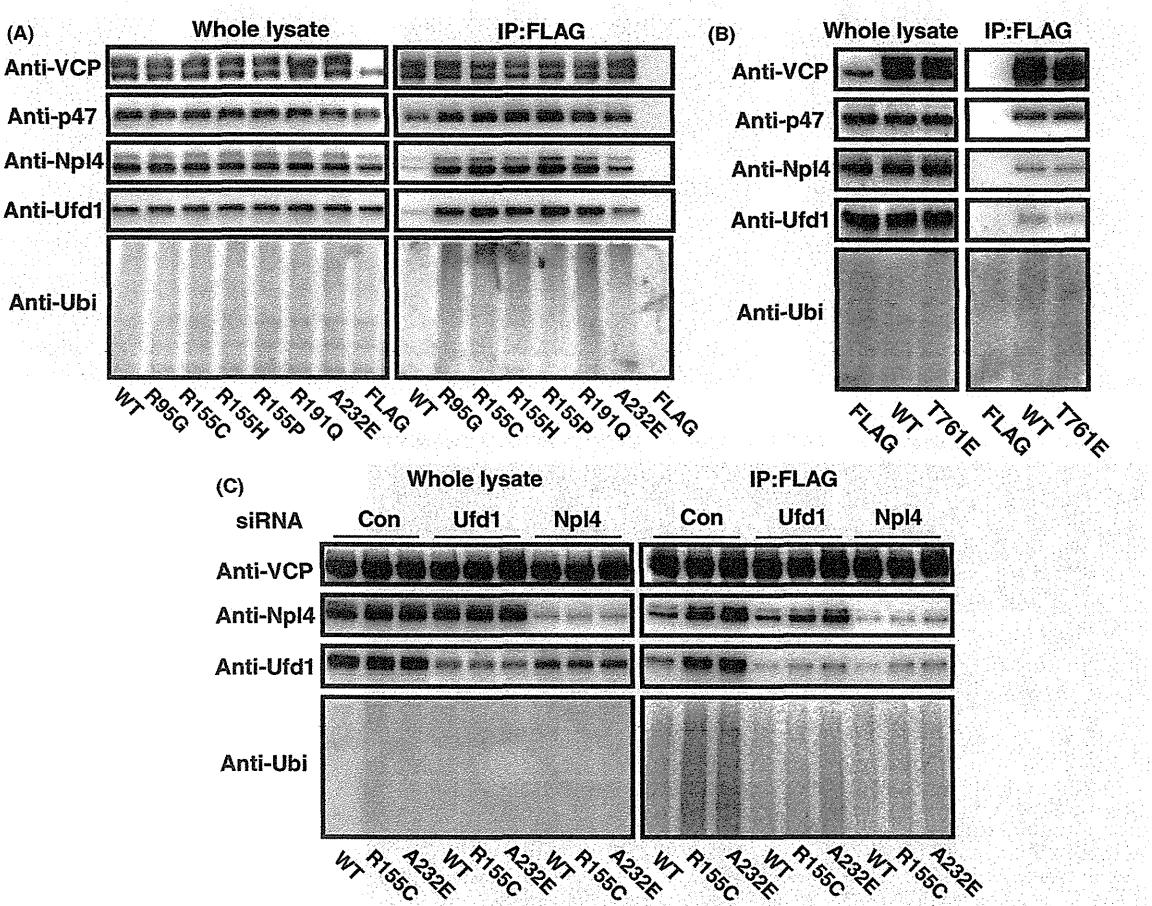

Figure 5 Enhanced cofactor-binding abilities of IBMPFD-VCPs. (A) Western blot analysis of VCP cofactors coimmunoprecipitated with FLAG-tagged wt-VCP or IBMPFD-VCPs. Immunoprecipitated VCP cofactors such as p47 (anti-p47), Npl4 (anti-Npl4) and Ufd1 (anti-Ufd1) or ubiquitinated proteins (anti-Ubi) were detected using specific antibodies (right panels). The whole cell lysates were also analyzed (left panels). (B) Western blot analysis of VCP cofactors coimmunoprecipitated with FLAG-tagged wt-VCP or VCP(T761E), as described in (A). (C) Western blot analysis of VCP cofactors coimmunoprecipitated with FLAG-tagged VCPs in cofactor knockdown cells. HEK293 cells were transfected with control siRNA, Ufd1 siRNA (216), Npl4 siRNA (679). Three days after transfection, FLAG-tagged VCPs were expressed for 1 day and analyzed as described in (A). IBMPFD, inclusion body myopathy associated with Paget disease of bone and frontotemporal dementia; VCP, valosin-containing protein.

proteins to IBMPFD-VCPs were enhanced with a help of Npl4 and Ufd1.

Phenotypes of IBMPFD-VCPs in *Drosophila* models

Finally, we examined the *in vivo* phenotypes of IBMPFD-VCPs by expressing IBMPFD-VCPs in fly eyes. Contrary to ter94 (*Drosophila* VCP) (Higashiyama *et al.* 2002), wt-VCP and all tested IBMPFD-VCPs as well as VCP(T761E) did not induce eye degenerations by themselves (Fig. 6A). However, by expression of wt-VCP with polyglutamines, the eye degenerations were mitigated (Koike *et al.* 2010). In contrast, VCP(T761E), VCP(R155H), VCP(R155P) and VCP(A232E), which all possessed elevated ATPase activities (Fig. 4C,D), worsened the polyglutamine-induced eye degenerations (Fig. 6A). Surprisingly, we

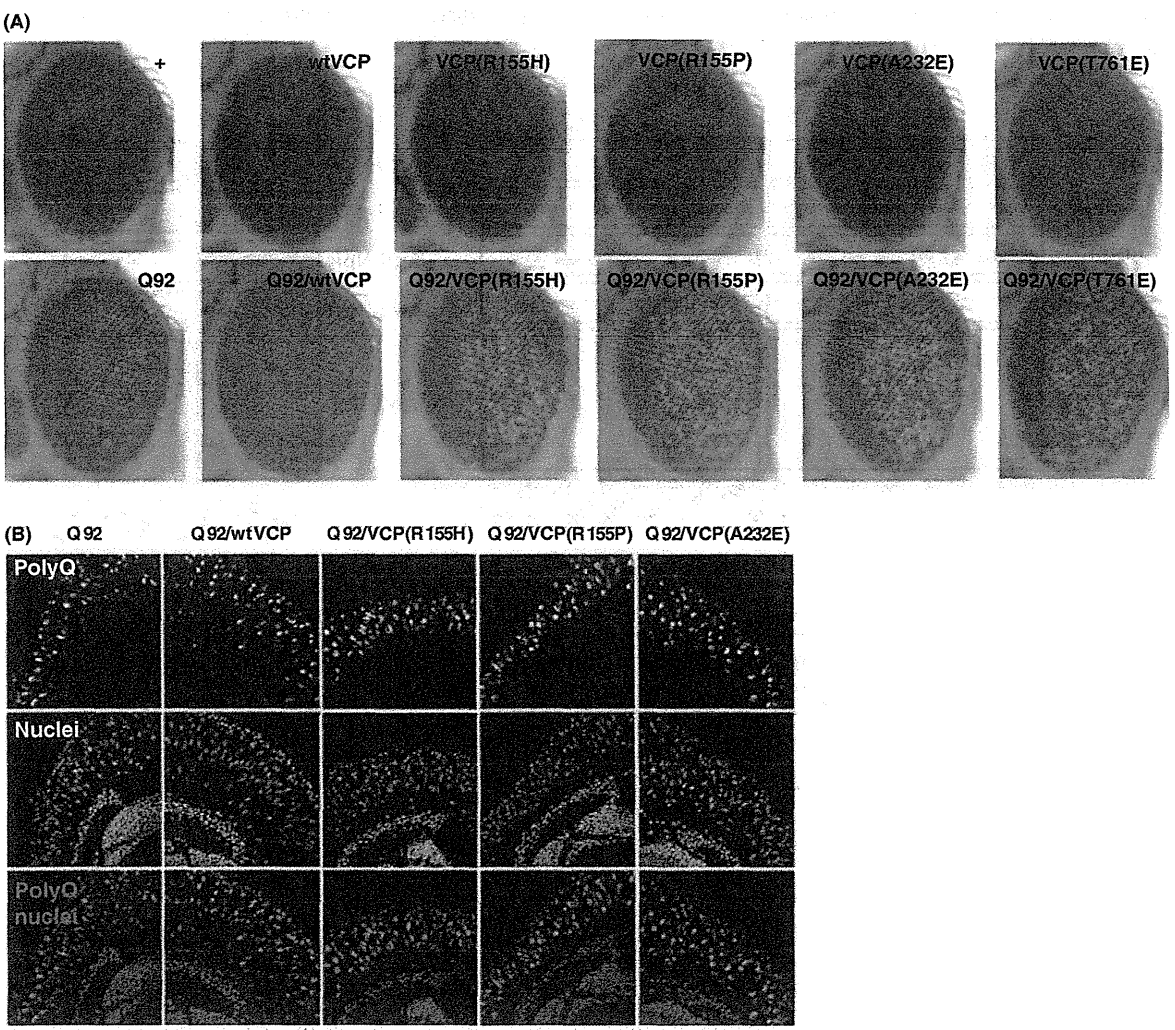

Figure 6 Effects of wt-VCP and mutant VCPs on eye degeneration and polyglutamine aggregate formation in *Drosophila*. (A) Light microphotographs of the compound eye from 5-day-old flies. wt-VCP and IBMPFD-VCPs and VCP(T761E) were expressed alone and together with FLAG-Q92 in *Drosophila* compound eyes (Higashiyama *et al.* 2002). (B) Confocal images of cryosections from 5-day-old fly heads. FLAG-Q92 was detected with anti-FLAG M5 antibody, and nuclei were stained with TOTO-3. In the overlay images, green indicates FLAG-Q92 and magenta indicates the nuclei. Genotypes of the flies are shown in the panels (A) or above the panels (B). IBMPFD, inclusion body myopathy associated with Paget disease of bone and frontotemporal dementia; VCP, valosin-containing protein.

could not observe apparent differences in sizes and frequencies of polyglutamine aggregates between eyes expressing wt-VCP and IBMPFD-VCPs (Fig. 6B).

Discussion

VCP colocalizes with abnormal protein aggregates observed in various neurodegenerative disorders (Hirabayashi *et al.* 2001; Mizuno *et al.* 2003; Ishigaki *et al.* 2004). We have recently showed that VCP functions as an aggregate-formase and/or as an aggregate-unfoldase (Kobayashi *et al.* 2007), but precise conditions or mechanisms that regulate either activity have remained to be clarified. In this study, we elucidated certain aspects of the aggregate-forming activity. We expressed VCP-GFP in the cells, treated the cells with proteasome inhibitors and then traced GFP signals via fluorescent time-lapse microscopy (Fig. 1B). VCP first appeared to bind abnormal proteins and formed several small aggregates throughout the cells and then carried them to the aggresome, vimentin-positive large aggregates (Johnston *et al.* 1998). Consistent with this, forced localization of VCP in the nucleus, by tagging NLS, created polyglutamine aggregates more frequently in the nucleus (Fig. 2). Although VCP usually colocalized with cytoplasmic polyglutamine aggregates, such colocalization was apparently destroyed in the nucleus in this cell culture experiment, suggesting that in the nucleus there may exist a protein(s) with affinity for abnormal proteins such as expanded polyglutamine much higher than that of VCP. VCP may hand out abnormal proteins to such a protein(s) in the nucleus. This possibility remains to be tested.

VCP colocalization with aggregates has been also observed in pathological samples of patients suffering from IBMPFD (Watts *et al.* 2004; Schröder *et al.* 2005). Given that VCP functions as an aggregate-formase or as an aggregate-unfoldase (Kobayashi *et al.* 2007), such colocalization is because of either elevated aggregate-formase activities or decreased aggregate-unfoldase activities in IBMPFD-VCPs. We indeed found that aggregate-forming activities were enhanced in IBMPFD-VCPs (Fig. 4A,B). This observation suggests that IBMPFD-VCPs make aggregates more efficiently than wt-VCP.

Biochemically, all immunopurified IBMPFD-VCPs showed significantly elevated ATPase activities, when compared with wt-VCP (Fig. 4C,D). Previously, it has been shown that ATPase activity of VCP(R155H) is normal by other group (Weihl *et al.* 2006). Indeed, elevation of the ATPase activities of VCP(R155H) was the lower than that of VCP(A232E), but was significantly higher than that of wild-type VCP in two different methods in our experiments (Fig. 4C,D). In addition, immunoprecipitation experiments demonstrated that IBMPFD-VCPs possessed elevated affinities for Ufd1 and Npl4, as well as for polyubiquitinated proteins (Fig. 5A). Either Ufd1 siRNA or Npl4 siRNA mostly abolished enhancement of IBMPFD-VCPs to bind the other partners and polyubiquitinated proteins (Fig. 5C). These results clearly showed that IBMPFD-VCPs, Ufd1 and Npl4 do bind polyubiquitinated proteins cooperatively. Consistent with this, the formation of polyglutamine aggregates was inhibited by VCP siRNA, Npl4 siRNA or Ufd1 siRNAs (Fig. 3). These results indicate that VCP, Ufd1 and Npl4, as a complex, were involved in forming abnormal protein aggregates.

The data presented in this study, collectively, indicated that IBMPFD-VCPs possess elevated ATPase activities (Fig. 4C,D) and enhanced abilities in binding to the cofactors, especially to Npl4 and Ufd1 as well as to polyubiquitinated proteins (Fig. 5A), leading to acceleration of abnormal protein aggregate formation in mammalian cells. Thus, we expected IBMPFD-VCPs to induce more polyglutamine aggregates in our fly models of polyglutamine disease, leading to more severe eye degenerations. This expectation was partly the case; co-expression of IBMPFD-VCPs enhanced polyglutamine-induced eye degenerations (Fig. 6A). But contrary to our expectation, levels of polyglutamine aggregates were not apparently affected by IBMPFD-VCPs in *Drosophila* eyes (Fig. 6B). This might be because of different nature of Ufd1 and Npl4 between mammals and *Drosophila*. Namely, IBMPFD-VCPs may possess elevated affinities for human Ufd1 and Npl4 but not for *Drosophila* Ufd1 or Npl4. This possibility remains to be tested.

Along with IBMPFD-VCPs, VCP(T761E) also enhanced the eye degenerations in a very similar way (Fig. 6A). These results indicated that in *Drosophila*, elevated ATPase activities of VCP are coupled profoundly with eye degenerations, but such pathogenic effects were only manifested in the presence of abnormal proteins such as polyglutamines, which is reminiscent of aging and could provide an explanation as to why IBMPFD is a late-onset disease. It is, however, currently unknown that similar situations are indeed applicable to the pathogenesis in human IBMPFD and its related disorders. But it is notable that among IBMPFD-VCPs, VCP(A232E) showed the highest ATPase activities (Fig. 4C,D), and it represented the severest clinical phenotypes (Watts *et al.* 2004). Further studies on VCP functions will

elucidate more detailed molecular mechanisms of human disorders with neurodegenerations, myopathy and bone disorders (Custer *et al.* 2010; Koike *et al.* 2010) and will lead to novel therapeutic hints on such currently noncurable disorders.

Experimental procedures

siRNAs

We tested three sets of siRNA for each mRNA and obtained essentially same results. Used siRNAs (VCP, Ufd1, Npl4, and p47 siRNAs) sequences were listed in Table S1 in supplement materials. All siRNA for the target proteins manifested essentially same phenotypes.

Antibodies and plasmids

The affinity-purified rabbit polyclonal anti-VCP, anti-p47, anti-Npl4 and anti-Ufd1 antibodies were developed previously (Noguchi *et al.* 2005). The following antibodies used in this study were purchased: mouse monoclonal anti-ubiquitin (Chemicon); mouse monoclonal anti-FLAG M5 (Sigma); mouse monoclonal anti-actin (Chemicon); rat monoclonal anti-GFP (Nacalai Tesque); mouse monoclonal anti-vimentin (V9) (Santa Cruz Biotechnology, Inc.); Alexa Fluor 488 goat anti-rat IgG and Alexa Fluor 594 goat anti-mouse IgG (Molecular Probes); donkey polyclonal anti-mouse IgG-HRP and anti-rabbit IgG-HRP (Amersham Biosciences). IBMPFD-associated VCP mutants expressing plasmid were constructed by site-directed mutagenesis. Plasmids encoding GFP-fused wt-VCP and various VCP mutants were constructed in pEGFP-N vector (Clontech).

Time-lapse imaging

For time-lapse imaging, HEK293 cells were seeded onto collagen-coated 35 -mm glass bottom dish (IWAKI). After attachment, cells were transfected with VCP-GFP expressing plasmids. Twelve hours after transfection, cells were treated with 1 μM MG132. After this treatment, cell morphologies and GFP signals were recorded during 24 h using an inverted fluorescence microscopy (Axiovert 200M; Carl Zeiss). Image analysis and processing were performed via the ZEISS AXIOVISION 4.5 software.

Quantification of aggregate formation

Approximately more than 500 randomly selected FLAG/GFP-positive cells per each sample were counted for aggregate formation by fluorescence microscopy (Axiovert 200M). Cells were scored positive if they contained one or several visible aggregates either in the cytoplasm or in the nucleus. Frequency of aggregate formation in transfected cells represents the percentage of the FLAG/GFP-positive cells that contained visible aggregates inside the cell.

Immunoprecipitation

For immunoprecipitation, HEK293 cells were transfected with a FLAG-VCP expression plasmid. One day after transfection, cells were harvested and lysed in 0.1% Triton lysis buffer. Each sample was mixed with anti-FLAG M2 Affinity Gel (Sigma), and stirred at 4 °C overnight. FLAG-VCP was eluted with FLAG-peptide (Sigma).

Measurement of ATPase activities

In this report, we measured ATPase activities of wt-VCP and various VCP mutants both by the molybdate assay and by the NADH-coupled assay. The procedures of both assays were as described previously (Kobayashi *et al.* 2002; Noguchi *et al.* 2005; Mori-Konya *et al.* 2009). In the molybdate assay, 500 ng of VCP protein was incubated in 20 μL of the ATPase assay buffer (20 mM HEPES (pH 7.4), 50 mM KCl, 5 mM $MgCl_2$) with 100 μM [γ-^{32}P]ATP (18.5GBq/mmol) (PerkinElmer) at 37 °C for 10 min. After incubation, the reaction was quenched by the addition of 200 μL of 7% ice-cold TCA solution with 1 mM K_2HPO_4, and then 50 μL of solution A (3.75% ammonium molybdate, 0.02 M silicotungstic acid in 3 N H_2SO_4) and 300 μL of *n*-butyl acetate were added to the reaction. The samples were mixed well and centrifuged at 12 000 ×*g* for 1 min. Then, 200 μL aliquots from the upper organic phases were taken, and their radioactivity was determined with a liquid scintillation counter for β-radiation, which determined the amounts of ^{32}P released. In the NADH-coupled assay, several different amounts of VCP proteins (1, 2, 5, and 10 μg) were preincubated at 37 °C for 10 min and then incubated with the ATPase assay buffer (50 mM Tris–HCl (pH 9.0), 150 mM NaCl, 2 mM $MgSO_4$), 3 mM phosphoenol pyruvate, 1 mM ATP, 0.25 mM NADH, 1.0 unit of pyruvate kinase and 1.5 units of lactate dehydrogenase. The absorbance of NADH was measured at 340 nm for 20 min at 37 °C.

Drosophila strain and genetics

Fly culture and crosses were performed at 25 °C on standard food. To generate UAS-mutant VCP flies, cDNAs of each mutant VCP were subcloned into BglII-NotI site of pUAST vector. Transgenic flies were generated by standard protocols. Several independent lines were established from each construct. GMR-Gal4 and GMR-FlagQ92 were described previously (Higashiyama *et al.* 2002).

Immunohistochemistry

Eye sections were incubated in 1 mg/mL RNase/PBS for 30 min at 37 °C and stained with 1 μM TOTO-3 (Invitrogen) at room temperature (RT) for 2 h. After TOTO-3 staining,

sections were incubated with anti-FLAG monoclonal antibody M5 (Sigma) at 1 : 1000 dilution in 5% skim milk/PBT at RT for 2 h. Then, sections were incubated with Alexa 488-labeled anti-mouse IgG antibody at 1 : 500 dilution in 5% skim milk/PBT at RT for 30 min and were analyzed by confocal microscopy (LSM510; Carl Zeiss).

Statistical analysis

Each experiment was conducted at least three times with consistent results. The gel or blot representative of each experiment is presented in this study. The statistical significance was analyzed using Student's *t*-test or Tukey's test.

Acknowledgements

We wish to thank K. Kuroiwa for technical assistance, our laboratory members for valuable discussions. This work was supported in part by research grants from the Ministry of Education, Culture, Sports, Science, and Technology of Japan.

References

Brunger, A.T. & DeLaBarre, B. (2003) NSF and p97/VCP: similar at first, difference at last. *FEBS Lett.* **555**, 126–133.

Custer, S.K., Neumann, M., Lu, H., Wright, A.C. & Taylor, J.P. (2010) Transgenic mice expressing mutant forms VCP/p97 recapitulate the full spectrum of IBMPFD including degeneration in muscle, brain and bone. *Hum. Mol. Genet.* **19**, 1741–1755.

Dalal, S. & Hanson, P.I. (2001) Membrane traffic: what drives the AAA motor? *Cell* **104**, 5–8.

Djamshidian, A., Schaefer, J., Haubenberger, D., Stogmann, E., Zimprich, F., Auff, E. & Zimprich, A. (2009) A novel mutation in the VCP gene (G157R) in a German family with inclusion-body myopathy with Paget disease of bone and frontotemporal dementia. *Muscle Nerve* **39**, 389–391.

Dreveny, I., Pye, V.E., Beuron, F., Briggs, L.C., Isaacson, R.L., Matthews, S.J., McKeown, C., Yuan, X., Zhang, X. & Freemont, P.S. (2004) p97 and close encounters of every kind: a brief review. *Biochem. Soc. Trans.* **32**, 715–720.

Forman, M.S., Mackenzie, I.R., Cairns, N.J., Swanson, E., Boyer, P.J., Drachman, D.A., Jhaveri, B.S., Karlawish, J.H., Pestronk, A., Smith, T.W., Tu, P.H., Watts, G.D., Markesbery, W.R., Smith, C.D. & Kimonis, V.E. (2006) Novel ubiquitin neuropathology in frontotemporal dementia with valosin-containing protein gene mutations. *J. Neuropathol. Exp. Neurol.* **65**, 571–581.

García-Mata, R., Bebök, Z., Sorscher, E.J. & Sztul, E.S. (1999) Characterization and dynamics of aggresome formation by a cytosolic GFP-chimera. *J. Cell Biol.* **146**, 1239–1254.

Haubenberger, D., Bittner, R.E., Rauch-Shorny, S., Zimprich, F., Mannhalter, C., Wagner, L., Mineva, I., Vass, K., Auff, E. & Zimprich, A. (2005) Inclusion body myopathy and Paget disease is linked to a novel mutation in the VCP gene. *Neurology* **65**, 1304–1305.

Higashiyama, H., Hirose, F., Yamaguchi, M., Inoue, Y.H., Fujikake, N., Matsukage, A. & Kakizuka, A. (2002) Identification of *ter94*, Drosophila *VCP*, as a modulator of polyglutamine-induced neurodegeneration. *Cell Death Differ.* **9**, 264–273.

Hirabayashi, M., Inoue, K., Tanaka, K., Nakadate, K., Ohsawa, Y., Kamei, Y., Popiel, A.H., Sinohara, A., Iwamatsu, A., Kimura, Y., Uchiyama, Y., Hori, S. & Kakizuka, A. (2001) VCP/p97 in abnormal protein aggregates, cytoplasmic vacuoles, and cell death, phenotypes relevant to neurodegeneration. *Cell Death Differ.* **8**, 977–984.

Hübbers, C.U., Clemen, C.S., Kesper, K., *et al.* (2007) Pathological consequences of VCP mutations on human striated muscle. *Brain* **130**, 381–393.

Ishigaki, S., Hishikawa, N., Niwa, J., Iemura, S., Natsume, T., Hori, S., Kakizuka, A., Tanaka, K. & Sobue, G. (2004) Physical and functional interaction between dorfin and valosin-containing protein that are colocalized in ubiquitylated inclusions in neurodegenerative disorders. *J. Biol. Chem.* **279**, 51376–51385.

Johnston, J.A., Illing, M.E. & Kopito, R.R. (2002) Cytoplasmic dynein/dynactin mediates the assembly of aggresomes. *Cell Motil. Cytoskeleton* **53**, 26–38.

Johnston, J.A., Ward, C.L. & Kopito, R.R. (1998) Aggresomes: a cellular response to misfolded proteins. *J. Cell Biol.* **143**, 1883–1898.

Ju, J.S., Fuentealba, R.A., Miller, S.E., Jackson, E., Piwnica-Worms, D., Baloh, R.H. & Weihl, C.C. (2009) Valosin-containing protein (VCP) is required for autophagy and is disrupted in VCP disease. *J. Cell Biol.* **87**, 875–888.

Ju, J.S., Miller, S.E., Hanson, P.I. & Weihl, C.C. (2008) Impaired protein aggregate handling and clearance underlie the pathogenesis of p97/VCP-associated disease. *J. Biol. Chem.* **283**, 30289–30299.

Kawaguchi, Y., Kovacs, J.J., McLaurin, A., Vance, J.M., Ito, A. & Yao, T.P. (2003) The deacetylase HDAC6 regulates aggresome formation and cell viability in response to misfolded protein stress. *Cell* **115**, 727–738.

Kawaguchi, Y., Okamoto, T., Taniwaki, M., Aizawa, M., Inoue, M., Katayama, S., Kawakami, H., Nakamura, S., Nishimura, M., Akiguchi, I., Kimura, J., Narumiya, S. & Kakizuka, A. (1994) CAG expansions in a novel gene for Machado-Joseph disease at chromosome 14q32.1. *Nat. Genet.* **8**, 221–228.

Kimonis, V.E., Kovach, M.J., Waggoner, B., Leal, S., Salam, A., Rimer, L., Davis, K., Khardori, R. & Gelber, D. (2000) Clinical and molecular studies in a unique family with autosomal dominant limb-girdle muscular dystrophy and Paget disease of bone. *Genet. Med.* **2**, 232–241.

Kimonis, V.E., Mehta, S.G., Fulchiero, E.C., Thomasova, D., Pasquali, M., Boycott, K., Neilan, E.G., Kartashov, A., Forman, M.S., Tucker, S., Kimonis, K., Mumm, S., Whyte, M.P., Smith, C.D. & Watts, G.D. (2008) Clinical studies in familial VCP myopathy associated with Paget disease of

bone and frontotemporal dementia. *Am. J. Med. Genet. A.* **146A**, 745–757.

Kimonis, V.E. & Watts, G.D. (2005) Autosomal dominant inclusion body myopathy, Paget disease of bone, and frontotemporal dementia. *Alzheimer Dis. Assoc. Disord.* **19**, S44–S47.

Kobayashi, T., Manno, A. & Kakizuka, A. (2007) Involvement of valosin-containing protein (VCP)/p97 in the formation and clearance of abnormal protein aggregates. *Genes Cells* **12**, 889–901.

Kobayashi, T., Tanaka, K., Inoue, K. & Kakizuka, A. (2002) Functional ATPase activity of p97/VCP is required for the quality control of endoplasmic reticulum in neuronally differentiated mammalian PC12 cells. *J. Biol. Chem.* **277**, 47358–47365.

Koike, M., Fukushi, J., Ichinohe, Y., Higashimae, N., Fujishiro, M., Sasaki, C., Yamaguchi, M., Uchihara, T., Yagishita, S., Ohizumi, H., Hori, S. & Kakizuka, A. (2010) Valosin-containing protein (VCP) in novel feedback machinery between abnormal protein accumulation and transcriptional suppression. *J. Biol. Chem.* in press.

Kovach, M.J., Waggoner, B., Leal, S.M., *et al.* (2001) Clinical delineation and localization to chromosome 9p13.3-p12 of a unique dominant disorder in four families: hereditary inclusion body myopathy, Paget disease of bone, and frontotemporal dementia. *Mol. Genet. Metab.* **74**, 458–475.

Mizuno, Y., Hori, S., Kakizuka, A. & Okamoto, K. (2003) Vacuole-creating protein in neurodegenerative diseases in humans. *Neurosci. Lett.* **343**, 77–80.

Mori-Konya, C., Kato, N., Maeda, R., Yasuda, K., Higashimae, N., Noguchi, M., Koike, M., Kimura, Y., Ohizumi, H., Hori, S. & Kakizuka, A. (2009) p97/valosin-containing protein (VCP) is highly modulated by phosphorylation and acetylation. *Genes Cells* **14**, 483–497.

Noguchi, M., Takata, T., Kimura, Y., Manno, A., Murakami, K., Koike, M., Ohizumi, H., Hori, S. & Kakizuka, A. (2005) ATPase activity of p97/valosin-containing protein is regulated by oxidative modification of the evolutionally conserved cysteine 522 residue in Walker A motif. *J. Biol. Chem.* **280**, 41332–41341.

Nowis, D., McConnell, E. & Wójcik, C. (2006) Destabilization of the VCP-Ufd1-Npl4 complex is associated with decreased levels of ERAD substrates. *Exp. Cell Res.* **312**, 2921–2932.

Schröder, R., Watts, G.D., Mehta, S.G., Evert, B.O., Broich, P., Fliessbach, K., Pauls, K., Hans, V.H., Kimonis, V. & Thal, D.R. (2005) Mutant valosin-containing protein causes a novel type of frontotemporal dementia. *Ann. Neurol.* **57**, 457–461.

Wang, Q., Song, C. & Li, C.C. (2004) Molecular perspectives on p97-VCP: progress in understanding its structure and diverse biological functions. *J. Struct. Biol.* **146**, 44–57.

Watts, G.D., Thomasova, D., Ramdeen, S.K., Fulchiero, E.C., Mehta, S.G., Drachman, D.A., Weihl, C.C., Jamrozik, Z., Kwiecinski, H., Kaminska, A. & Kimonis, V.E. (2007) Novel VCP mutations in inclusion body myopathy associated with Paget disease of bone and frontotemporal dementia. *Clin. Genet.* **72**, 420–426.

Watts, G.D., Wymer, J., Kovach, M.J., Mehta, S.G., Mumm, S., Darvish, D., Pestronk, A., Whyte, M.P. & Kimonis, V.E. (2004) Inclusion body myopathy associated with Paget disease of bone and frontotemporal dementia is caused by mutant valosin-containing protein. *Nat. Genet.* **36**, 377–381.

Weihl, C.C., Dalal, S., Pestronk, A. & Hanson, P.I. (2006) Inclusion body myopathy-associated mutations in p97/VCP impair endoplasmic reticulum-associated degradation. *Hum. Mol. Genet.* **15**, 189–199.

Weihl, C.C., Pestronk, A. & Kimonis, V.E. (2009) Valosin-containing protein disease: inclusion body myopathy with Paget's disease of the bone and fronto-temporal dementia. *Neuromuscul. Disord.* **19**, 308–315.

Zhang, X., Shaw, A., Bates, P.A., Newman, R.H., Gowen, B., Orlova, E., Gorman, M.A., Kondo, H., Dokurno, P., Lally, J., Leonard, G., Meyer, H., van Heel, M. & Freemont, P.S. (2000) Structure of the AAA ATPase p97. *Mol. Cell* **6**, 1473–1484.

Received: 8 February 2010
Accepted: 12 May 2010

Supporting Information/Supplementary material

The following Supporting Information can be found in the online version of the article:

Table S1 List of siRNA sequences used in this work

Video S1 Time-lapse analysis of aggresome formation in cells expressing GFP-tagged VCP.

Additional Supporting Information may be found in the online version of this article.

Please note: Wiley-Blackwell are not responsible for the content or functionality of any supporting materials supplied by the authors. Any queries (other than missing material) should be directed to the corresponding author for the article.

nature neuroscience

ARTICLES

Ontogeny-recapitulating generation and tissue integration of ES cell–derived Purkinje cells

Keiko Muguruma[1], Ayaka Nishiyama[1], Yuichi Ono[2], Hiroyuki Miyawaki[3], Eri Mizuhara[2], Seiji Hori[4], Akira Kakizuka[4], Kunihiko Obata[5], Yuchio Yanagawa[6,7], Tomoo Hirano[3] & Yoshiki Sasai[1]

Purkinje cells are the sole output neurons of the cerebellar cortex and their dysfunction causes severe ataxia. We found that Purkinje cells could be robustly generated from mouse embryonic stem (ES) cells by recapitulating the self-inductive signaling microenvironments of the isthmic organizer. The cell-surface marker Neph3 enabled us to carry out timed prospective selection of Purkinje cell progenitors, which generated morphologically characteristic neurons with highly arborized dendrites that expressed mature Purkinje cell–specific markers such as the glutamate receptor subunit GluRδ2. Similar to mature Purkinje cells, these neurons also showed characteristic spontaneous and repeated action potentials and their postsynaptic excitatory potentials were generated exclusively through nonNMDA glutamate receptors. Fetal transplantation of precursors isolated by fluorescence-activated cell sorting showed orthotopic integration of the grafted neurons into the Purkinje cell layer with their axons extending to the deep cerebellar nuclei and dendrites receiving climbing and parallel fibers. This selective preparation of bona fide Purkinje cells should aid future investigation of this important neuron.

During embryonic development, the cerebellar anlage arises from two distinct tissues in dorsal rhombomere 1 adjacent to the fourth ventricle[1–3]: the cerebellar ventricular zone, which expresses the basic helix-loop-helix (bHLH) transcription factor Ptf1a, and the rhombomere 1 rhombic lip, which expresses another bHLH factor, Math1. The Ptf1a$^+$ progenitors produce GABAergic neurons of the cerebellar cortex (Purkinje, basket, stellate and Golgi neurons) and of the deep cerebellar nuclei (DCN)[4]. In contrast, Math1$^+$ progenitors generate cerebellar glutamatergic neurons, including granule cells and large DCN projection neurons[5–7].

The initial phase of cerebellar development depends on the formation and function of the isthmic organizer[8], which lies at the midbrain-hindbrain boundary (MHB). This organizer is formed by the intricate regulatory functions of region-specific transcription factors such as En1/2, Pax2/5/8, Otx2 and Gbx2 (refs. 8–11). The expression of these factors is under the control of fibroblast growth factor 8 (Fgf8) secreted by the isthmic organizer itself[9–11]. Mutant mice with reduced *Fgf8* expression have a severe defect in cerebellar development[12], whereas Fgf8 misexpression in the chick brain forms ectopic cerebellar tissues[13]. Following the onset of Fgf8 expression, the expression of another key signaling factor, Wnt1, starts in the MHB. These two factors form a positive autofeedback loop to drive each other's expression that also involves the expression of transcription factors such as En2 and Pax2 (refs. 14–16). In addition, Fgf8 and Wnt1 act as organizer factors that pattern the tissues around the MHB. This self-inducing feature of isthmic organizer development presumably contributes to its potent patterning ability and to the robust maintenance of its tissue identity after ectopic transplantation to other brain regions.

Among the cerebellar neurons, Purkinje cells have a central role in integrating heterogeneous neural inputs from the mossy and climbing fibers. Purkinje cell dysfunction (hereditary or acquired) leads to severe motor discoordination. Math1$^+$ granule cell progenitors are generated from ES cells at a relatively high efficiency (>15%) in serum-free suspension culture (serum-free culture of embryoid body–like aggregates or SFEB[17]) in the presence of bone morphogenetic protein (BMP) and Wnt signals[18]. In contrast, although ES cells can be induced to differentiate into Purkinje cells when treated with Fgf8 and Wnt ligands, their production is quite inefficient, with Purkinje cells typically comprising less than 1% of the total[18–20].

Therefore, we took a different strategy that focuses on the initiation of the endogenous program for self-inducing isthmic development and successfully applied it to the efficient differentiation of ES cells into functional Purkinje cells, using a modified SFEB culture (SFEBq)[21,22].

RESULTS

Transient Fgf treatment induces isthmus/rhombomere 1 tissues

Although *En2* is initially expressed in a broad domain of the mes- and metencephalon, during early cerebellar development (embryonic day (E)12.5), En2 (clearly detectable by immunofluorescence) is strongly expressed mainly in the MHB and its neighboring regions[8,23] (the isthmic/rhombomere 1 (Otx2$^-$) region and the caudal-most midbrain region, just rostral to the isthmus (Otx2$^+$; **Fig. 1a**)). Hereafter, these En2$^+$ tissues are referred as MHB-proximity tissues.

[1]Organogenesis and Neurogenesis Group, RIKEN Center for Developmental Biology, Kobe, Japan. [2]Group for Neuronal Differentiation, KAN Institute, Kobe, Japan. [3]Department of Biophysics, Graduate School of Science, Kyoto University, Kyoto, Japan. [4]Laboratory of Functional Biology, Graduate School of Biostudies, Kyoto University, Kyoto, Japan. [5]Obata Research Unit, RIKEN Brain Science Institute, Wako, Japan. [6]Department of Genetic and Behavioral Neuroscience, Gunma University Graduate School of Medicine, Maebashi, Japan. [7]Japan Science and Technology Agency, CREST, Tokyo, Japan. Correspondence should be addressed to Y.S. (yoshikisasai@cdb.riken.jp).

Received 12 July; accepted 13 August; published online 12 September 2010; doi:10.1038/nn.2638

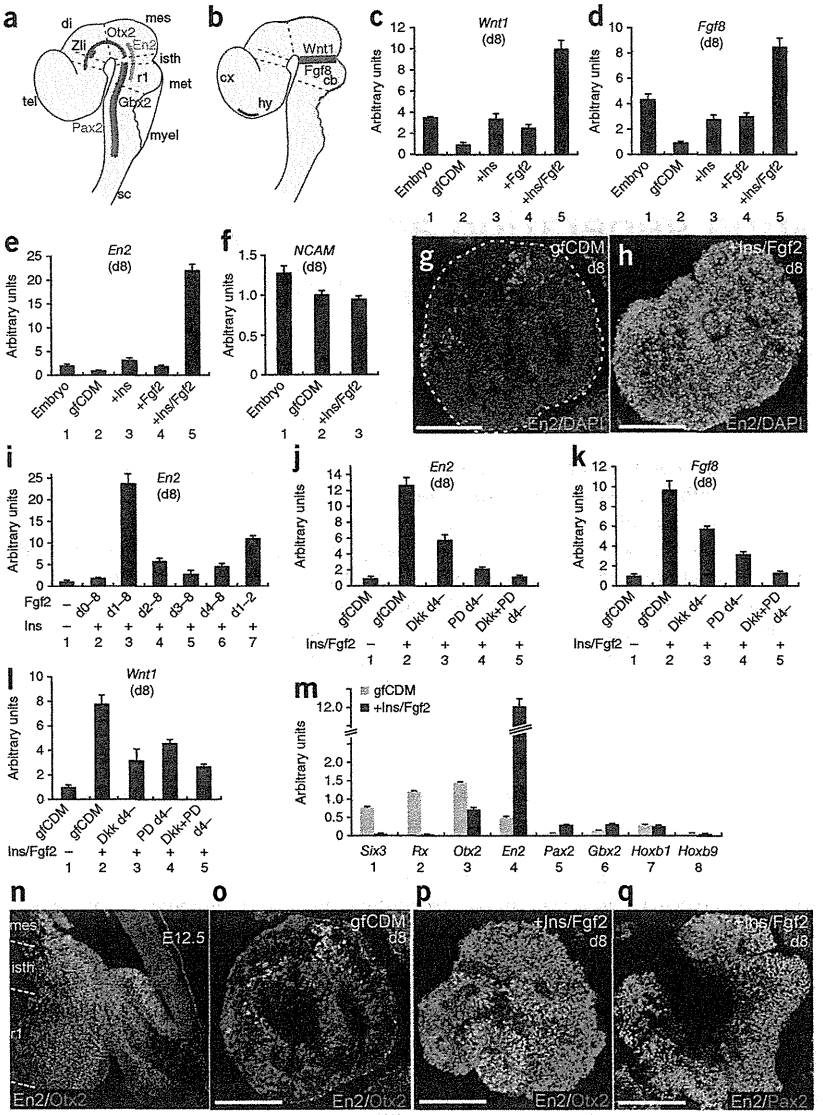

Figure 1 Fgf2 and insulin cooperatively induce generation of midbrain-hindbrain identity in ES cells in SFEBq culture. (**a**,**b**) Expression of markers in the embryonic neural tube (E12.5 mouse). (**a**) Otx2 (red), En2 (green), Gbx2 (blue) and Pax2 (purple). (**b**) *Wnt1* (red) and *Fgf8* (blue). As well as the MHB region, Wnt1 is expressed in the dorsal-most domain of the neural tube and Fgf8 is expressed in the rostral forebrain. (**c**–**f**) qPCR analysis of SFEBq-cultured ES cell aggregates on day 8 for the expression of *Wnt1* (**c**), *Fgf8* (**d**), *En2* (**e**) and *NCAM* (**f**) ($n = 120$ aggregates from 5 independent experiments). Total RNA from E11.5 whole embryos (lane 1) was used as a control. (**g**,**h**) Cryosections of SFEBq-cultured ES cell aggregates on day 8. ES cells were cultured in gfCDM alone (**g**) or containing insulin and Fgf2 (**h**). Sections were immunostained with anti-En2 antibody and counterstained with DAPI. Broken white line shows outline of an aggregate. (**i**–**m**) qPCR analysis of SFEBq-cultured ES cell aggregates on day 8 for the expression of *En2* (**i**,**j**), *Fgf8* (**k**), *Wnt1* (**l**) and regional markers along the rostral-caudal axis (**m**) ($n = 140$ aggregates from 5 independent experiments). Dkk (250 ng ml^{-1}) and/or PD173074 (10 nM) were added to culture on day 4. (**n**) Sagittal section of mouse mesencephalon/metencephalon at E12.5, immunostained with antibodies to En2 and Otx2. (**o**–**q**) Cryosections of SFEBq-cultured ES cell aggregates on day 8. ES cells were cultured in gfCDM alone (**o**) or containing insulin and Fgf2 (**p**,**q**). Sections were immunostained with antibodies to En2 (**o**–**q**), Otx2 (**o**,**p**) and Pax2 (**q**). tel, telencephalon; di, diencephalon; mes, mescencephalon; met, metencephalon; myel, myelencephalon; sc, spinal cord; isth, isthmus; rhombomere 1, rhombomere 1; cx, cortex; hy, hypothalamus; cb, cerebellum. Scale bars, 100 μm. Error bars represent s.e.m.

When totally growth factor–free, chemically defined medium (gfCDM)[21] is used, ES cell aggregates cultured in the SFEBq method selectively differentiate into rostral forebrain tissues that express the forebrain-specific transcription factors Six3 and Rx[21], but not into En2$^+$ tissues. We first investigated the effects of Fgf8 and Wnt signals, which are expressed in the MHB-proximity region (**Fig. 1b**), on the induction of En2. However, the percentage of En2$^+$ cells did not exceed 15% of total cells on day 8 under any of the conditions tested (up to 200 ng ml^{-1}), suggesting that MHB development can be only partly recapitulated *in vitro* by exogenous Fgf8 and Wnt. With this in mind, we employed a different strategy that makes use of endogenous Fgf8 and Wnt1 as local organizing factors.

Previous results suggest that the addition of insulin (on days 0–8) has a moderate caudalizing activity, particularly when added to gfCDM culture[21]. Indeed, insulin treatment suppressed the expression of *Six3* and *Rx* (**Supplementary Fig. 1**), and moderately increased the expression of *Wnt1*, *Fgf8* and *En2* (<3-fold on day 8; **Fig. 1c–e**). There is evidence that Fgf2 has rhombomere 1–inducing activity in an embryonic neural explant assay[24]. Consistent with this, when Fgf2 (20 ng ml^{-1}) was added to the culture from day 1 along with insulin, the expression of *Wnt1* and *Fgf8* was substantially induced on both day 8 (eight- and ten-fold, respectively; **Fig. 1c,d**) and day 5 (**Supplementary Fig. 1**). The synergistic effect of Fgf2 and insulin on *En2* expression was particularly high (20-fold on day 8; **Fig. 1e**) whereas general neural differentiation was unaffected (**Fig. 1f**). The majority (>80%) of cells in the SFEBq aggregates were strongly immunoreactive for En2 on day 8 (**Fig. 1g,h**). Thus, treatment with Fgf2 and insulin promoted *Wnt1* and *Fgf8* expression and induced nearly selective differentiation into En2$^+$ tissues. Fgf2 was at least twice as effective at inducing the expression of *En2* and *Fgf8* than Fgf4, 5 or 8 when added to culture on day 1 (**Supplementary Fig. 1**).

We did not observe clear En2 induction when the Fgf2 treatment was started on day 0 (instead of day 1), showing that its addition on day 0 has an inhibitory effect (**Fig. 1i**). In contrast, even transient Fgf2 treatment from day 1 to day 2 was sufficient to substantially induce En2$^+$ tissues (**Fig. 1i**). Fgf2 treatment on days 2–8 was substantially less effective than on days 1–8 (**Fig. 1i**). Given that neural differentiation starts around day 3 in SFEBq culture[21] (the cells instead express epiblast markers during days 1–3; data not shown), the main role of Fgf2 was probably to confer selective competence on differentiating ES cell aggregates before neural differentiation,

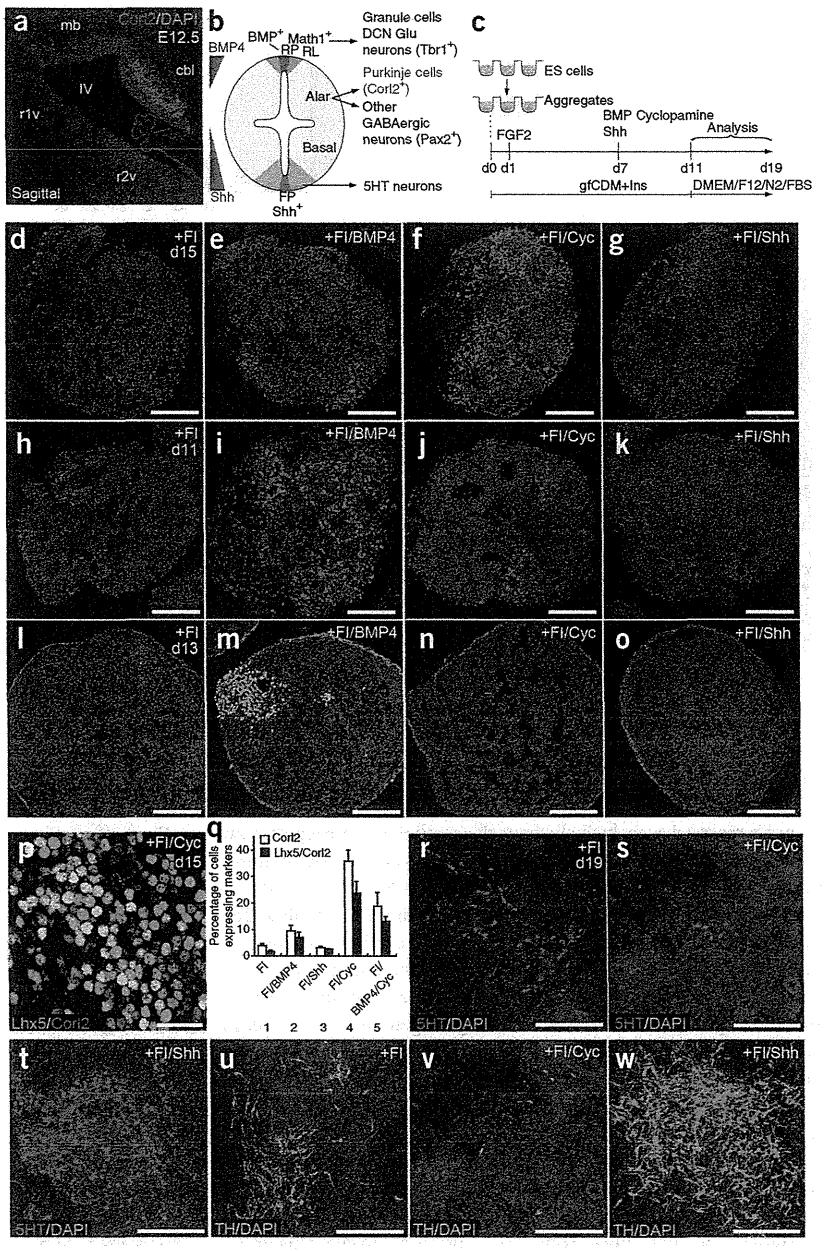

Figure 2 Sequential treatment of Fgf2 and a Shh inhibitor in the presence of insulin induces cerebellar plate precursors in SFEBq culture. (**a**) Expression of Corl2 (red) in a sagittal section of mouse hindbrain. Cells of the cerebellar plate express Corl2. (**b**) Schematic diagram showing dorsal-ventral patterning of the rostral hindbrain. (**c**) Procedure for ES cell culture. BMP4 (1 nM), Shh (30 nM) or cyclopamine (10 μM) was added on day 7. (**d–o**) Sections of ES cell aggregates treated with Fgf2 (**d,h,l**), Fgf2 and BMP4 (**e,i,m**), Fgf2 and cyclopamine (**f,j,n**), or Fgf2 and Shh (**g,k,o**). The cells were immunostained with antibodies to Corl2 on day 15 (**d–g**), Math1 on day 11 (**h–k**) or Tbr1 on day 13 (**l–o**). Nuclei were counterstained with DAPI. (**p**) Expression of Lhx5 and Corl2 in ES cell aggregate treated with Fgf2 and cyclopamine. (**q**) Percentage of cells positive for Corl2 (open) and double-positive for Lhx5 and Corl2 (closed) in ES cell aggregates ($n = 24$ aggregates from three independent experiments). (**r–w**) Differentiation of 5HT-positive (**r–t**) and tyrosine hydroxylase–positive (**u–w**) neurons by treatment with Fgf2 (**r,u**), Fgf2 and cyclopamine (**s,v**) and Fgf2 and Shh (**t,w**). RP, roof plate; FP, floor plate; mb, midbrain; cbl, cerebellar plate; r1v, ventral region of rhombomere 1; r2v, ventral region of rhombomere 2; IV, fourth ventricle. Scale bars: 100 μm (**d–o**); 200 μm (**p–u**); 25 μm (**w**). Error bars represent s.e.m.

and to bias the cells' differentiation toward midbrain-hindbrain regionality. In addition, the increased expression of *En2*, *Fgf8* and *Wnt1* was inhibited by the late addition of the Fgf inhibitor PD173074 or the Wnt inhibitor Dkk1 (day 4 onwards; **Fig. 1j–l**). This result supports the idea that the endogenous isthmic organizer factors Fgf8 and Wnt1 (or related proteins) were induced as a secondary effect of the transient Fgf2 treatment (in the presence of insulin), and that their activities are essential for the induction of En2 and the maintenance of their own expression *in vitro*, as *in vivo*.

The coordinated control of regional marker expression in SFEBq culture with Fgf2 and insulin (FI) treatment (SFEBq/FI) was also confirmed by qPCR analysis. Forebrain markers (*Six3*, *Rx* and *Otx2*) were suppressed, and MHB-proximity markers (*En2*, *Pax2* and *Gbx2*) were increased, but there was little effect on more caudal markers (*Hoxb1* and *b9*; **Fig. 1m**).

In the embryonic brain (E12), Otx2 is expressed in both the forebrain and midbrain, but not in the hindbrain or isthmus (**Fig. 1n**). At this stage, En2 is coexpressed with Otx2 exclusively in the caudal-most midbrain (yellow in **Fig. 1n**), but not in the isthmus/rhombomere 1 region (green). SFEBq/gfCDM–cultured aggregates, which rarely contained En2$^+$ cells, mostly consisted of Otx2$^+$/En2$^-$ cells (**Fig. 1o**), consistent with their forebrain-dominant nature[21]. In contrast, SFEBq/FI–cultured aggregates contained few Otx2$^+$/En2$^-$ cells (<5%). The majority of the cells (>70%) were Otx2$^-$/En2$^+$ (isthmus/rhombomere 1 type), and 10–20% of the En2$^+$ cells coexpressed Otx2 (caudal midbrain type) (**Fig. 1p** and **Supplementary Fig. 1**). These findings suggested that a substantial population of the En2$^+$ cells that were induced in SFEBq/FI culture had regional characteristics of the isthmus/rhombomere 1. Concordantly, ~60% of the En2$^+$ cells coexpressed Pax2 (**Fig. 1q** and **Supplementary Fig. 1**), which colocalizes with En2 *in vivo* only in the embryonic isthmic/rhombomere 1 region but not in the midbrain area (**Supplementary Fig. 1**). These findings indicate that the SFEBq/FI culture supports the efficient and selective differentiation of ES cell–derived neural progenitors into En2$^+$ tissues, particularly with isthmus/rhombomere 1 characteristics (**Supplementary Fig. 1**).

Cerebellar precursors specified by passive dorsalization

The transcriptional corepressor Corl2 (**Fig. 2a,b**) is a very early Purkinje cell marker (E12 onwards) that is not expressed in other

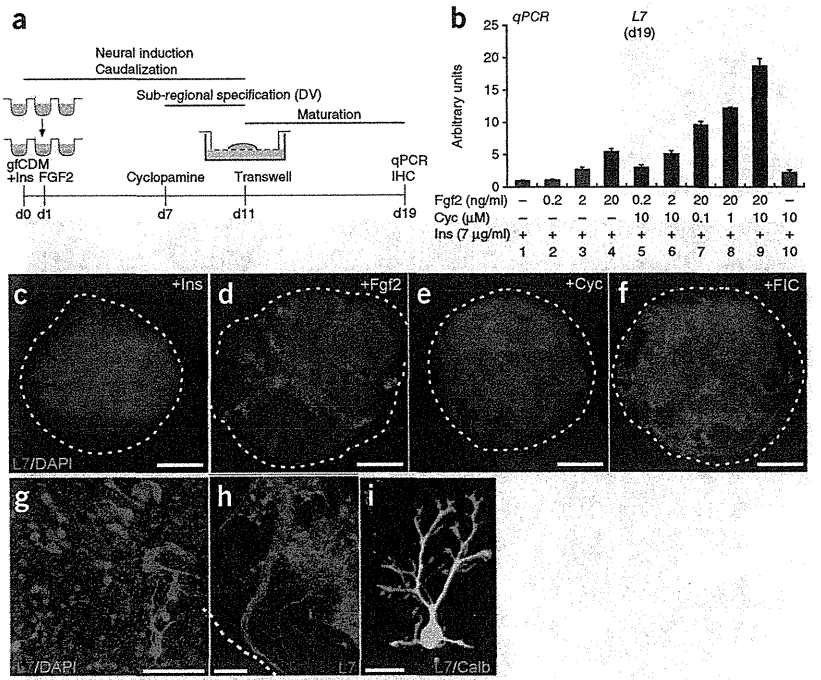

Figure 3 Generation of Purkinje cells in SFEBq/FIC culture in Transwell culture. **(a)** Procedure for the differentiation of Purkinje cells from ES cell culture. Treated aggregates were cultured on a Transwell membrane and analyzed on day 19. **(b)** qPCR analysis of *L7* expression by ES cell aggregates treated with different concentrations of Fgf2 and cyclopamine ($n = 140$ aggregates from 5 independent experiments). **(c–f)** Aggregates were treated with insulin **(c)**, Fgf2 **(d)**, cyclopamine **(e)** or all three (FIC; **f**) and immunostained for L7. Aggregates are outlined by a broken white line. **(g–j)** High-magnification view of aggregates treated with insulin + Fgf2 + cyclopamine. **(h)** Fasciculated L7-positive axons run in the aggregate. White broken line demarcates the outline of the aggregate. **(i)** A cell co-expressing L7 and calbindin extends dendrites, showing a typical Purkinje cell morphology. Scale bars: 150 μm **(c–f)**; 50 μm **(g)**; 100 μm **(h)**; 20 μm **(i)**. Error bars represent s.e.m.

cerebellar neurons[25]. Using Corl2 as an indicator, we searched for conditions to optimize Purkinje cell precursor generation by modifying dorsal-ventral specification (**Fig. 2c–o**).

During early cerebellar development (E10–11 for mouse), Purkinje cell precursors arise exclusively from the cerebellar neuroepithelium on the alar plate of rhombomere 1, which subsequently contributes to the genesis of the cerebellar plate[3] (light blue in **Fig. 2b**). The dorsal tip of the rhombomere 1 alar plate forms the rhombic lip (**Fig. 2b**), which generates the Math1$^+$ granule cells of the cerebellar cortex and the DCN glutamatergic neurons positive for the transcriptional factor Tbr1 (ref. 7). The basal plate of rhombomere 1 develops into the main body of the pons, and its ventral-most region generates serotonergic (5HT$^+$) neurons. Midbrain dopaminergic neurons expressing tyrosine hydroxylase arise just rostrally to this region.

BMP signals, which emanate from the roof plate (**Fig. 2b**), have an inductive function in the dorsal specification of rhombomere 1 tissues[26]. In contrast, sonic hedgehog (Shh) derived from the floor plate promotes neural ventralization[24,27]. Treatment with BMP4 on days 7–11 induced the expression of the dorsal-most neuronal markers Math1 and Tbr1 (**Figs. 2i,m**; Tbr1$^+$ neurons always clustered). These cells also expressed Pax6, which is a marker for granule cells, and Meis1 and 2, which are DCN markers (**Supplementary Fig. 2**). However, BMP4 did not substantially increase the number of Corl2$^+$ cells (**Fig. 2e**).

We therefore took an alternative approach, to promote dorsalization indirectly. Cyclopamine antagonizes hedgehog receptors, thereby shutting off the ventralizing effect of endogenous Shh in ES cell aggregates. As we hoped, cyclopamine treatment (days 7–11) caused a marked increase in the Corl2$^+$ population (35.7 ± 4.5% of total cells) in SFEBq/FI culture (**Fig. 2f**), but not in the Math1$^+$ or Tbr1$^+$ populations (**Fig. 2j,n**). Three-quarters of Corl2$^+$ precursors coexpressed Lhx5, another marker for Purkinje cell precursors (**Fig. 2p,q**). Combined treatment with BMP4 and cyclopamine did not increase the percentage of Corl2$^+$ cells (18.9 ± 5.1%; **Fig. 2q**) or Math1$^+$ cells (**Supplementary Fig. 2**).

As expected, Shh was clearly detectable in the SFEBq/FI aggregates by qPCR on day 8 (data not shown). In addition, the differentiation of 5HT$^+$ and tyrosine hydroxylase–positive neurons (which are Shh-dependent *in vivo*) in the aggregate was completely inhibited by cyclopamine, whereas exogenous Shh treatment markedly increased the number of 5HT$^+$ and tyrosine hydroxylase–positive neurons (**Fig. 2r–w**), without promoting the expression of Corl2, Math1 or Tbr1 (**Fig. 2g,k,o**). The anti-ventralizing (passive dorsalization) effect of cyclopamine was confirmed by the qPCR analysis of dorsoventral marker expression (**Supplementary Fig. 2**). Cyclopamine treatment suppressed the basal plate markers *Nkx2.2*, *Nkx6.1* and *Olig2* and elevated the expression of the dorsal markers *Pax7* and *Corl2*, whereas the intermediate dorsoventral marker *Dbx2* and the dorsal-most marker *Zic1* were mostly unaffected. These findings indicate that Corl2$^+$ Purkinje cell–like precursors are efficiently produced in SFEBq/FI culture with the additional anti-ventralizing effect of cyclopamine (SFEBq/FIC, hereafter).

Efficient differentiation of Purkinje cells

We cultured SFEBq/FIC aggregates en bloc on a porous membrane (Transwell culture[21,22] during days 11–19; **Fig. 3a**) to neuronal maturation in long-term culture. The combination of cyclopamine and Fgf2 (**Fig. 3b–f**) efficiently induced the differentiation of Purkinje cells expressing the lineage-specific marker L7 in the ES cell–derived neural tissues (42.6 ± 5.2% of total neurons; **Fig. 3f**). A qPCR analysis showed that *L7* induction was about 20-fold more efficient under these conditions than with insulin treatment alone (**Fig. 3b**). Within these neural tissues, most L7$^+$ cells were found in clusters (**Fig. 3f,g**), and their axons frequently formed long fascicles that extended circumferentially at the periphery of the tissues (**Fig. 3h**). On day 19, L7$^+$ cells were positive for calbindin and Corl2 (**Fig. 3i** and data not shown).

Exposure to cyclopamine on days 7–8 was sufficient to promote L7$^+$ cell differentiation (**Supplementary Fig. 3**) and to shut off endogenous *Shh* expression (not shown). In contrast, Fgf2 treatment was most effective for *L7* induction from days 1–11. It was ~50% and 10% as efficient, respectively, when added from days 1–4 or days 4–11 (**Supplementary Fig. 3**). Fgf4 and Fgf8 (days 1–11) also qualitatively promoted *L7* expression in the presence of insulin and cyclopamine, but not as efficiently as Fgf2 at 20 ng ml^{-1} (**Supplementary Fig. 3**)

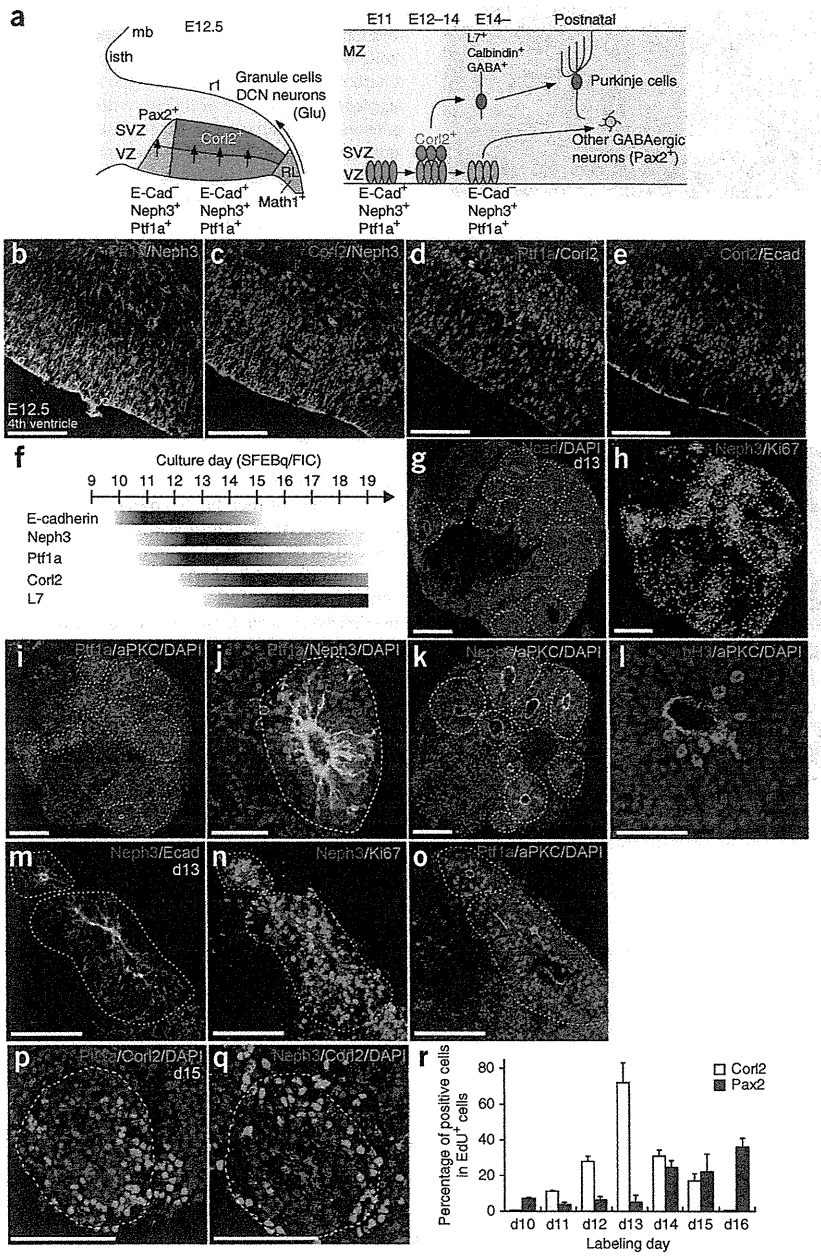

Figure 4 ES cell–derived neuroepithelial rosettes express cerebellar progenitor markers in SFEBq culture. (**a**) Schematic diagram showing the organization of the cerebellar plate (left, sagittal view) and the ontogenesis of cerebellar neurons (right). (**b–e**) Expression of cerebellar progenitor markers in the E12.5 mouse cerebellar plate. Neph3 (**b**,**c**), E-cadherin (**e**) and Ptf1a (**b**,**d**) were expressed in the mitotic neuroepithelium, whereas Corl2 (**c–e**) was expressed in postmitotic cells. (**f**) Temporal expression of the markers in ES cell aggregates in SFEBq/FIC culture. (**g–i**) Adjacent sections of an aggregate on day 13, immunostained for N-cadherin (**g**), Neph3 and Ki67 (**h**) or Ptf1a and aPKC (**i**). Neural rosettes are demarcated by broken white lines. (**j**) High-magnification view of a Ptf1a$^+$ Neph3$^+$ neural rosette on day 13. (**k**) An aggregate on day 13, immunostained for Neph3 and aPKC. Neph3 was preferentially enriched at the aPKC$^+$ apical surface. (**l**) High-magnification view of a neural rosette on day 13, immunostained with pH3 and aPKC. (**m–o**) High-magnification view of adjacent sections of an aggregate on day 13, immunostained with Neph3 and E-cadherin (**m**), Neph3 and Ki67 (**n**) or Ptf1a and aPKC (**o**). (**p**,**q**) Adjacent sections of an aggregate on day 15, immunostained with Ptf1a and Corl2 (**p**) or Neph3 and Corl2 (**q**). (**r**) Percentage of EdU-positive cells expressing Corl2 (open columns) and Pax2 (closed columns) in aggregates on the indicated days ($n = 56$ aggregates from 3 independent experiments). Scale bars: 100 μm (**b–e**,**g–i**,**k**,**m–q**); 50 μm (**l**,**j**). Error bars represent s.e.m.

or 100 ng ml^{-1} (data not shown). The addition of Wnt decreased the induction of *L7* in SFEBq/FIC culture (**Supplementary Fig. 3**). Collectively, the timed treatment with insulin (day 0 onwards), Fgf2 (day 1 onwards) and cyclopamine (day 7 onwards) in SFEBq culture steered ES cells to sequentially acquire a neural fate, rhombomere 1/MHB regional identity and cerebellar plate characteristics, which together led to efficient Purkinje cell differentiation *in vitro*.

Recapitulation of early cerebellar plate development

In the early cerebellar primordium, the neuroepithelium begins to express tissue-specific marker genes on E11–E12. One such marker is Ptf1a, a transcription factor that is essential for the genesis of Purkinje cells and cerebellar GABAergic interneurons (**Fig. 4a,b**). The membrane molecule Neph3 is the product of a Ptf1a target gene[28]. *Ptf1a* and *Neph3* are expressed together in most of the cerebellar plate neuroepithelium (**Fig. 4b**), but not at the Math1$^+$ rhombic lip (**Fig. 4a**, left). The mouse cerebellar plate neuroepithelium gives rise to Purkinje cells and cerebellar GABAergic interneurons at distinct developmental stages: E11–E13 for Purkinje cells and E13–P15 for GABAergic interneurons[29,30]. Postmitotic Purkinje cell precursors become positive for the lineage-specific marker Corl2 while still in the subventricular zone (SVZ; **Figs. 4a** and **3c,d**). The cerebellar plate neuroepithelium coexpresses Corl2 and E-cadherin (with N-cadherin) with a spatiotemporal pattern that overlaps with Purkinje cell generation (E12–14)[28] (**Fig. 4e**).

The temporal expression pattern of Purkinje cell differentiation markers in SFEBq/FIC culture resembled the *in vivo* expression pattern (**Fig. 4f**). For instance, obvious *Neph3*$^+$ expression was induced on day 11 in a cyclopamine-dependent manner (**Supplementary Fig. 2**). On day 13 of SFEBq/FIC culture, a large number of N-cadherin$^+$ neural cells were still mitotic (Ki67$^+$) in culture (**Fig. 4g,h**), and a large portion of these cells formed characteristic epithelial-sphere structures (neural rosettes). Of these neural rosettes, 73.0 ± 6.6% were double-positive for Neph3 and Ptf1a (**Fig. 4h–j** and **Supplementary Fig. 4**). Each neural rosette had a fixed epithelial apico-basal polarity, with the apical side to the interior of the rosette and demarcated by strong N-cadherin and aPKC expression (**Fig. 4g,k**). High mitotic